note, the viability of ScN2a cells measured with WST-8 assay was not reduced up to 5-fold higher concentrations than EC_{99} of rPrP-Q218K (Figure 1C). On the contrary, quinacrine reduced viability of ScN2a cells by 50% at the concentration of EC_{99} (1.5 μM) (Figure 2C). As previously demonstrated[13,14], quinacrine inhibited PrP^{Sc} formation in ScN2a cells (EC_{50}=0.45 μM, EC_{99}= 1.5 μM) but less efficiently.

When both rPrP-Q218K and quinacrine were applied onto ScN2a cells simultaneously, an additive inhibitory effect was observed. After the combined administration of 0.5 μM of quinacrine and 0.22 μM (5 μg/ml) of rPrP-Q218K, PrP^{Sc} formation in ScN2a cells was reduced by another 30% compared with quinacrine alone (Figure 2A, 2B). When combined with 0.43 μM (10 μg/ml) of rPrP-Q218K, EC_{99} of quinacrine was also decreased from 1.5 μM to 0.5 μM, in which the cell viability was recovered from 50% to over 90% as inversely proportional to the concentration of quinacrine (Figure 2C).

In order to gain further mechanistic insight into the inhibition of PrP^{Sc} formation by rPrP-Q218K, morphological and biochemical analyses were performed. Indirect immunofluorescent microscopy detected these rPrPs on the cell surface with no difference in distribution profiles (Figure 3). These results show that some factor/s other than the GPI-anchor rendered the rPrPs detected on the cell surface.

SPR measurement revealed that both analytes of rPrP-Q218K and rPrP-WT did not bind to rPrP-WT immobilized onto the chip surface as a ligand, whereas anti-prion mAb 6H4 bound the ligand of rPrP at the equilibrium dissociation constant (K_D) of 2.2 x 10^{-9}. In order to correct the instrumental noise and non-specific binding, the sensorgram of the flow cell containing rPrP-WT-immobilized sensor chip was subtracted from that of a blank cell. However, SPR could not detect any interaction between amine-coupled rPrP-WT on the surface of the chip and soluble rPrP-Q218K/rPrP-WT in the flow, indicating their KD values below the detection limit of SPR measurement.

Discussion

While mouse Q218K in a GPI-anchored form has already been known as a dominant negative in ScN2a culture cells[6,7] and transgenic mice[8], we have demonstrated that the administration of non-GPI-anchored rPrP-Q218K sufficiently inhibits PrP^{Sc} formation in ScN2a cells for the first time.

Meier *et al.* recently reported that soluble wild-type PrP derivatives might represent a new class of prion replication antagonists with transgenic and gene knockout approaches[15]. In PrP transgenic mice with a wild-type background, the expression of PrP^{C} rendered soluble and dimeric by fusion to immunoglobulin Fcγ (PrP-Fc2) delays PrP^{Sc} accumulation, agent replication, and onset of disease following inoculation with infective prions. While it is preliminary to consider such gene therapeutics, *e.g.* an *ex vivo* gene transfer approach[16,17], the direct administration of soluble rPrPs such as our rPrP-Q218K would be an alternative approach for prion therapeutics. In addition, homogeneous and high-quality soluble rPrP-Q218K could be easily prepared from large-scale fermentation of *E. coli* in sufficient quantities.

Artificial administration of anti-PrP antibodies have been shown to exert a protective effect against infection with PrP^{Sc} [18, 19], which is in good agreement with our own data *in vitro*; EC_{50} of anti-PrP antibody Fab D18 (kindly provided by Dr. Stanley B. Prusiner)=6 nM, and EC_{99}=30 nM (data not shown). However, a recent clinical trial of Aβ vaccination targeting Alzheimer's disease has been halted due to the serious neurological complications of autoimmune reactions developing in

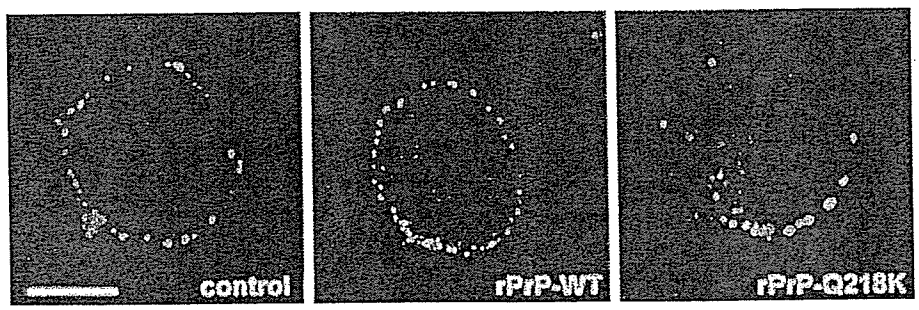

FIGURE 3: Both rPrP-WT and rPrP-218K bind to N2a cells. N2a cells are incubated for 3 h with PBS(–), 10 μg/ml rPrP-WT or rPrP-Q218K, washed with PBS(–), fixed with 2% formalin, and subjected to indirect immunofluorescent microscopy. rPrPs, asialo-GM1 are displayed in green and red, respectively. PrP^{C} and asialo-GM1 are localized on the plasma membrane. Both rPrPs are detected on a part of lipid rafts. Bar: 15 μm.

some patients[20,21]. In contrast, the generation of anti-PrP antibodies *in vivo* has proven quite difficult in wild-type animals, PrP being a notoriously poor immunogen[22]. From the aspect of avoiding such unwanted autoimmune reactions, rPrPs might also be considered as a better candidate for prion therapeutics.

Quinacrine, an anti-malarial drug, was reported to inhibit PrP^{Sc} formation in ScN2a cells[13,14], and has already been prescribed for CJD patients in a tentative way[23]. Unfortunately, quinacrine tends to provoke a drug-induced liver dysfunction[24], which frequently forces cessation of the drug administration. In order to minimize the side effects of quinacrine, we expected that combination treatment of multiple anti–prion drugs might be an alternative option. In fact, when combined with rPrP-Q218K, the EC_{99} of quinacrine was successfully reduced and no significant cytotoxicity was observed at the same range of concentration in ScN2a cells. Such a combination could alleviate the side effects of quinacrine by reducing its effective concentration without changing or even accelerating the inhibition efficacy.

Enari *et al.*[25] proposed that sequestration of PrP^{C} by anti-PrP antibody or removal by phosphatidyl-inositol specific phospholipase C (PIPLC) leads to depletion of PrP^{Sc} due to much more rapid turnover of PrP^{Sc} than previously supposed. Since decrease in PrP^{C} by administration of rPrP-Q218K to ScN2a cells was not detected (Figure 1A), the inhibition of PrP^{Sc} accumulation seems to be caused by secession of PrP^{Sc} synthesis, stimulation of PrP^{Sc} degradation or a combination of both.

It was shown that both rPrP-Q218K and rPrP-WT in non-GPI-anchored form were equally detectable on the cell surface, where the conversion of PrP^{C} into PrP^{Sc} takes place[26,27]. Of note, such equal binding seems to be independent of the inhibition of PrP^{Sc} formation, since only rPrP-Q218K but not rPrP-WT exclusively inhibited the PrP^{Sc} formation in ScN2a cells. Nonetheless, one might assume that rPrP-Q218K aberrantly binds to endogenous PrP^{C} in terms of the binding partner, which is undetectable by the conventional immunofluorescent microscopy, and concurrently inhibits PrP^{Sc} formation. Real-time kinetics analysis by SPR, however, failed to detect any significant difference in the binding kinetics of rPrP-WT as a ligand with rPrP-WT or rPrP-Q218K as analytes. Measurements of on-rates (ka) and off-rates (kd) of protein-protein interactions made by SPR is extremely sensitive, and these values are directly related to KD[28]. Taken into account the fact that SPR successfully detects binding interactions in the order of 10^{-3}~$^{-4}$ of KD[28], it seems less likely that such discrepancy between rPrP-Q218K and rPrP-WT on the PrP^{Sc} inhibition could be explained by the different binding kinetics of these rPrPs against PrP, although rPrP may not perfectly substitute for PrP^{C}. Instead, it seems likely that these rPrPs more readily interact with a binding factor/s other than PrP where rPrP-Q218K and rPrP-WT are equally detected but inhibit PrP^{Sc} formation differently. Legname *et al.*[29] recently reported that the dominant-negative MoPrP (MoPrP-Q218K)-Fc, in which the C-terminus of MoPrP was fused to the Fc portion of an IgG, not only binds to granule cells but also binds to neurons of the molecular layer where PrP^{C} is expressed, and assuming that the cells of the molecular layer express an auxiliary protein/s, provisionally designated protein X[6,30], which is involved in prion replication. Identification of such factor/s remains to be further examined.

Acknowledgments

We thank Drs. Naoko Iwanami, Yuko Nakamura, and Ken'ichi Hagiwara for useful discussions and Dr. Tamaki Muramoto for providing ScN2a culture cells. This work was supported in part by grants from the Ministry of Health, Labor and Welfare of Japan (14161301), and Core Research for Evolutional Science and Technology (CREST), Japan Science and Technology Corporation.

References

1 Prusiner SB (2001). Shattuck lecture—neurodegenerative diseases and prions. *N Engl J Med* **344**, 1516-1526
2 Collinge J (1999). Variant Creutzfeldt-Jakob disease. *Lancet* **354**, 317-323
3 Prusiner SB (1998). Prions. *Proc Natl Acad Sci USA* **95**, 13363-13383
4 Kitamoto T and Tateishi J (1994). Human prion diseases with variant prion protein. *Philos Trans R Soc Lond B* **343**, 391-398
5 Shibuya S, Higuchi J, Shin RW, Tateishi J and Kitamoto T (1998). Codon 219 Lys allele of PRNP is not found in sporadic Creutzfeldt-Jakob disease. *Ann Neurol* **43**, 826-828
6 Kaneko K, Zulianello L, Scott M, Cooper CM, Wallace AC, James TL, Cohen FE and Prusiner SB (1997). Evidence for protein X binding to a discontinuous epitope on the cellular prion protein during scrapie prion propagation. *Proc Natl Acad Sci USA* **94**, 10069-10074
7 Zulianello L, Kaneko K, Scott M, Erpel S, Han D, Cohen FE and Prusiner SB (2000). Dominant-negative inhibition of prion formation diminished by deletion mutagenesis of the prion protein. *J Virol* **74**, 4351-4360
8 Perrier V, Kaneko K, Safar J, Vergara J, Tremblay P, DeArmond SJ, Cohen FE, Prusiner SB and Wallace AC (2002). Dominant-negative inhibition of prion replication in transgenic mice. *Proc Natl Acad Sci USA* **99**,13079-13084

9 Scott MR, Köler R, Foster D and Prusiner SB (1992). Chimeric prion protein expression in cultured cells and transgenic mice. *Protein Sci* **1**, 986-997

10 Rogers M, Serban D, Gyuris T, Scott M, Torchia T and Prusiner SB (1991). Epitope mapping of the Syrian hamster prion protein utilizing chimeric and mutant genes in a vaccinia virus expression system. *J Immunol* **147**, 3568-3574

11 Butler DA, Scott MA, Bockman JM, Borchelt DR, Taraboulos A, Hsiao KK, Kingsbury DT and Prusiner SB (1988). Scrapie-infected murine neuroblastoma cells produce protease-resistant prion proteins. *J Virol* **62**, 1558-1564

12 Korth C, Kaneko K and Prusiner SB (2000). Expression of unglycosylated mutated prion protein facilitates PrP(Sc) formation in neuroblastoma cells infected with different prion strains. *J Gen Virol* **81**, 2555-2563

13 Doh-Ura K, Iwaki T and Caughey B (2000). Lysosomotropic agents and cysteine protease inhibitors inhibit scrapie-associated prion protein accumulation. *J Virol* **74**, 4894-4897

14 Korth C, May BCH, Cohen FE and Prusiner SB (2001). Acridine and phenothiazine derivatives as pharmacotherapeutics for prion disease. *Proc Natl Acad Sci USA* **98**, 9836-9841

15 Meier P, Genoud N, Prinz M, Maissen M, Rulicke T, Zurbriggen A, Raeber AJ and Aguzzi A (2003). Soluble dimeric prion protein binds PrP(Sc) *in vivo* and antagonizes prion disease. *Cell* **113**, 49-60

16 Corbel SY and Rossi FM (2002). Latest developments and in vivo use of the Tet system: ex vivo and in vivo delivery of tetracycline-regulated genes. *Curr Opin Biotechnol* **13**, 448-452

17 Kapturczak MH, Flotte T and Atkinson MA (2001). Adeno-associated virus (AAV) as a vehicle for therapeutic gene delivery: improvements in vector design and viral production enhance potential to prolong graft survival in pancreatic islet cell transplantation for the reversal of type 1 diabetes. *Curr Mol Med* **1**, 245-258

18 Peretz D, Williamson RA, Kaneko K, Vergara J, Leclerc E, Schmitt-Ulms G, Mehlhorn IR, Legname G, Wormald MR, Rudd PM, Dwek RA, Burton DR and Prusiner SB (2001). Antibodies inhibit prion propagation and clear cell cultures of prion infectivity. *Nature* **412**, 739-743

19 White AR, Enever P, Tayebi M, Mushens R, Linehan J, Brandner S, Anstee D, Collinge J and Hawke S (2003). Monoclonal antibodies inhibit prion replication and delay the development of prion disease. *Nature* **422**, 80-83

20 Dodart JC, Bales KR and Paul SR (2003). Immunotherapy for Alzheimer's disease: will vaccination work? *Trends Mol Med* **9**, 85-87

21 McGeer PL and McGeer E (2003). Is there a future for vaccination as a treatment for Alzheimer's disease? *Neurobiol Aging* **24**, 391-395

22 Koller MF, Grau T and Christen P (2002). Induction of antibodies against murine full-length prion protein in wild-type mice. *J Neuroimmunol* **132**, 113-116

23 Follette P (2003). New perspectives for prion therapeutics meeting. Prion disease treatment's early promise unravels. *Science* **299**, 191-192

24 Scoazec JY, Krolak-Salmon P, Casez O, Besson G, Thobois S, Kopp N, Perret-Liaudet A and Streichenberger N (2003). Quinacrine-induced cytolytic hepatitis in sporadic Creutzfeldt-Jakob disease. *Ann Neurol* **53**, 546-547

25 Enari M, Flechsig E and Weissmann C (2001). Scrapie prion protein accumulation by scrapie-infected neuroblastoma cells abrogated by exposure to a prion protein antibody. . *Proc Natl Acad Sci USA* **98**, 9295-9299

26 Taraboulos A, Scott M, Semenov A, Avrahami D, Laszlo L and Prusiner SB (1995). Cholesterol depletion and modification of COOH-terminal targeting sequence of the prion protein inhibit formation of the scrapie isoform. *J Cell Biol* **129**, 121-132

27 Kaneko K, Vey M, Scott M, Pilkuhn S, Cohen FE and Prusiner SB (1997). COOH-terminal sequence of the cellular prion protein directs subcellular trafficking and controls conversion into the scrapie isoform. *Proc Natl Acad Sci USA* **94**, 2333-2338

28 Myszka DG (1997). Kinetic analysis of macromolecular interactions using surface plasmon resonance biosensors. *Curr Opin Biotechnol* **8**, 50-57

29 Legname G., Nelken P, Guan Z, Kanyo ZF, DeArmond SJ and Prusiner SB (2002). Prion and doppel proteins bind to granule cells of the cerebellum. *Proc Natl Acad Sci USA* **99**, 16285-16290

30 Telling GC, Scott M, Mastrianni J, Gabizon R, Torchia M, Cohen FE, DeArmond SJ and Prusiner SB (1995). Prion propagation in mice expressing human and chimeric PrP transgenes implicates the interaction of cellular PrP with another protein. *Cell* **83**, 79-90

BIOLOGY OF REPRODUCTION 71, 515–521 (2004)
Published online before print 14 April 2004.
DOI 10.1095/biolreprod.104.027565

Developmental Regulation of Ubiquitin C-Terminal Hydrolase Isozyme Expression During Spermatogenesis in Mice

Jungkee Kwon,[2,3] Yu-Lai Wang,[1] Rieko Setsuie,[3,4] Satoshi Sekiguchi,[2] Mikako Sakurai,[3,4] Yae Sato,[3,4] Won-Woo Lee,[2] Yoshiyuki Ishii,[2] Shigeru Kyuwa,[2] Mami Noda,[4] Keiji Wada,[3] and Yasuhiro Yoshikawa[1,2]

Department of Biomedical Science,[2] Graduate School of Agricultural and Life Sciences, University of Tokyo, Bunkyo-ku, Tokyo, 113-8657, Japan
Department of Degenerative Neurological Disease,[3] National Institute of Neuroscience, National Center of Neurology and Psychiatry, Kodaira, Tokyo, 187-8502, Japan
Laboratory of Pathophysiology,[4] Graduate School of Pharmaceutical Sciences, Kyushu University, Higashi-ku, Fukuoka, 812-8582, Japan

ABSTRACT

The ubiquitin pathway functions in the process of protein turnover in eukaryotic cells. This pathway comprises the enzymes that ubiquitinate/deubiquitinate target proteins and the proteasome that degrades ubiquitin-conjugated proteins. Ubiquitin C-terminal hydrolases (UCHs) are thought to be essential for maintaining ubiquitination activity by releasing ubiquitin (Ub) from its substrates. Mammalian UCH-L1 and UCH-L3 are small proteins that share considerable homology at the amino acid level. Both of these UCHs are highly expressed in the testis/ovary and neuronal cells. Our previous work demonstrated that UCH-L1-deficient gracile axonal dystrophy (*gad*) mice exhibit progressively decreasing spermatogonial stem cell proliferation, suggesting that UCH isozymes in the testis function during spermatogenesis. To analyze the expression patterns of UCH isozymes during spermatogenesis, we isolated nearly homogeneous populations of spermatogonia, spermatocytes, spermatids, and Sertoli cells from mouse testes. Western blot analysis detected UCH-L1 in spermatogonia and Sertoli cells, whereas UCH-L3 was detected in spermatocytes and spermatids. Moreover, reverse transcription-polymerase chain reaction analysis of UCH isozymes showed that UCH-L1 and UCH-L4 mRNAs are expressed in spermatogonia, whereas UCH-L3 and UCH-L5 mRNAs are expressed mainly in spermatocytes and spermatids. These results suggest that UCH-L1 and UCH-L3 have distinct functions during spermatogenesis, namely, that UCH-L1 may act during mitotic proliferation of spermatogonial stem cells whereas UCH-L3 may function in the meiotic differentiation of spermatocytes into spermatids.

male reproductive tract, meiosis, Sertoli cells, spermatogenesis, testis

INTRODUCTION

Ubiquitination of proteins is mediated by specific enzymes, namely E1 (ubiquitin-activating), E2 (ubiquitin-conjugating), and E3 (ubiquitin ligase) [1]. In this pathway, polyubiquitinated proteins are translocated to the proteasome and proteolytically degraded in an energy-dependent manner. The ubiquitin pathway plays important roles in regulating numerous cellular processes, including the degradation of intracellular proteins, cell-cycle regulation, stress responses, and programmed cell death [2–6]. Ubiquitin can be released from polyubiquitin chains or ubiquitin-protein conjugates via the action of deubiquitinating enzymes. These enzymes are divided into two families: ubiquitin C-terminal hydrolases (UCHs) and ubiquitin-specific proteases (UBPs). UCHs remove ubiquitin from peptides or small C-terminal ubiquitin adducts only, whereas UBPs are thought to disassemble polyubiquitin chains [7, 8].

Recent studies show that there are at least four mammalian UCH isozymes, among which the residues surrounding the active site share a high degree of homology [8, 9]. Mouse *Uchl1* and *Uchl3* encode proteins of similar size that share 52% amino acid sequence identity [8, 10]. However, the distribution of these isozymes is quite distinct; UCH-L1 mRNA is selectively and highly expressed in the testis/ovary and neuronal cells [10–12], whereas UCH-L3 mRNA is expressed in all tissues, including the testis/ovary and brain [13, 14]. UCH-L1-specific antibodies stain the testis, especially spermatogonia and Sertoli cells [15–18]. In addition, UCH-L1-deficient gracile axonal dystrophy (*gad*) mutant mice exhibit pathological changes, such as progressively decreasing spermatogonial stem cell proliferation [18]. These results led us to postulate that UCH isozymes in the testis function in the development of spermatogonia into mature sperm. Spermatogenesis is a complex, highly organized process that is divided into three phases: proliferation, meiosis, and spermiogenesis [19], each of which may require the activity of specific UCH isozymes. However, our understanding of the functional roles and the localization of UCH isozymes during spermatogenesis is limited.

In the present study, we generated peptide-specific antibodies against sequences within UCH-L1 or UCH-L3 and purified developing sperm cells at each stage from testes using immunomagnetic beads followed by discontinuous Percoll gradient centrifugation [20–23]. We found that the expression level of each UCH isozyme increased during the first round of spermatogenesis, and that the isozymes exhibited differential expression in the mouse testis [24]. Our results suggest that UCH isozymes play an important role in the regulation of spermatogenesis.

[1]Correspondence: Yasuhiro Yoshikawa, Department of Biomedical Science, Graduate School of Agricultural and Life Sciences, University of Tokyo, 1-1-1 Yayoi, Bunkyo-ku, Tokyo 113-8657, Japan.
FAX: 81 3 5841 8186; e-mail: ayyoshi@mail.ecc.u-tokyo.ac.jp

Received: 20 January 2004.
First decision: 5 February 2004.
Accepted: 19 March 2004.

ISSN: 0006-3363. http://www.biolreprod.org

MATERIALS AND METHODS

Animals

The *gad* [11] and *Uchl3* knockout [13] mice were used as controls. The *gad* mouse is an autosomal recessive mutant that was obtained from the cross between CBA and RFM mice. The mutant line was maintained by intercross for more than 20 generations. The *Uchl3* knockout mouse was generated by the standard method using homologously recombinant ES cells from 129SV mice. The knockout line was back-crossed several times to C57BL/6J mice. Male Balb/c mice were purchased from Nihon CLEA, Inc. (Tokyo, Japan), and all animals were maintained at the National Institute of Neuroscience, National Center of Neurology and Psychiatry (Japan).

All mouse experiments were performed in accordance with the institution's regulations for animal care and with the approval of the Animal Investigation Committee.

Isolation of Type A Spermatogonia and Sertoli Cells

Sequential enzymatic digestion of testicular tubules was performed as previously described [21]. After treatment with erythrocyte lysing buffer, testes from ten 2-wk-old and two 8-wk-old Balb/c mice were incubated twice for 5 min at 34°C with medium containing 0.5 mg/ml collagenase IV-S (Sigma-Aldrich, St. Louis, MO) and digested for 10 min at 34°C with medium containing 1 mg/ml trypsin (Sigma-Aldrich).

After the sequential enzymatic digestion, type A spermatogonia were isolated using immunomagnetic beads. The cells were incubated at room temperature for 15 min with biotin-conjugated rat anti-mouse CD117 (1 μg/10^6 cells), which recognizes the extracellular domain of the c-kit receptor (clone 2B8; Pharmingen, San Diego, CA). The cell suspension was then centrifuged at 300 × *g* for 5 min and washed with Dulbecco modified Eagle medium to remove excess antibody. The cell pellet was then resuspended in 80 μl buffer and incubated with 20 μl MACS anti-biotin microbeads (Miltenyi Biotec, Bergisch Gladbach, Germany) per 10^7 total cells at 6–12°C for 15 min. The cell suspension was then washed carefully and resuspended in 500 μl buffer per 10^8 total cells. The c-kit-positive cells (type A spermatogonia) were separated with a MACS separator (Miltenyi Biotec) and collected. The suspension containing Sertoli cells was resuspended at a concentration of 1 × 10^6 cells/ml in tissue culture medium containing 10% fetal calf serum.

Sertoli Cell Culture and Purification

The suspension containing Sertoli cells obtained from testes of ten 2-wk-old mice was plated on lectin- (Datura stramonium agglutinin; Sigma, St. Louis, MO) coated dishes as described [25, 26] and incubated for 3 days at 37°C. Alkaline phosphatase activity was visualized according to the procedure of Cox and Singer [27]. Cultured cells were incubated in reaction buffer (100 mM Tris-HCl, 100 mM NaCl, 50 mM $MgCl_2$, pH 9.5) containing 0.17 mg/ml 5-bromo-4-chloro-3-indolyl phosphate and 0.33 mg/ml nitro blue tetrazolium chloride.

Isolation of Spermatocytes and Spermatids

After isolating type A spermatogonia from testes of 8-wk-old mice using immunomagnetic beads, the testicular cell suspension was separated by discontinuous Percoll (Amersham Biosciences, Piscataway, NJ) gradient centrifugation [20]. The recovered cell populations were analyzed by phase-contrast microscopy [28], fluorescence-activated cell sorting (FACS) [29], and reverse transcription-polymerase chain reaction (RT-PCR).

RT-PCR Analysis of Isolated Cells Expressing Specific Marker Genes

From each population of spermatogonia, spermatocytes, spermatids, and Sertoli cells isolated from testicular cell suspensions, mRNAs were extracted using the QuickPrep micro mRNA purification kit (Amersham Biosciences) and subjected to reverse transcription with a first-strand cDNA synthesis kit (Amersham Biosciences) according to the manufacturer's instructions. PCR was performed with the following primers; c-kit [30], 5′-AAGATTTGCGATTTCGGGC-3′ and 5′-CTGAAAATGCTCTC TGGTGCC-3′; Histone H1t [7], 5′-GTCCAGCTCTTGACCATGTCG-3′ and 5′-GCTTTTTCCCTCGCCTTTTAG-3′; SP-10 [31], 5′-TTTATCTG CTTGGATCTGCCC-3′, and 5′-GCTTGAAAGTTGCTGAACCG-3′; stem cell factor (SCF) [32], 5′-ATAGGAAAGCCGCAAAGGC-3′ and 5′-TTACAAGCGAAATGAGAGCCG-3′; and glyceraldehyde-3-phosphate dehydrogenase [33]. Each sample was amplified using the AmpliTaq Gold GeneAmp system (Applied Biosystems, Foster City, CA).

FACS Analysis of Isolated Cells

FACS analysis was performed as described by Malkove et al. [29, 34]. Briefly, isolated spermatogenic cells were fixed in 70% ethanol overnight at 4°C and then incubated in propidium iodide staining solution (50 μg/ml and 100 U/ml RNase A in PBS) for 30 min at room temperature. Within 2 h poststaining, the isolated spermatogenic cells were analyzed by FACS (FACSCalibur, Becton Dickinson, Franklin Lakes, NJ). Excitation was at 488 nm and emission was at ~600 nm.

Quantitative mRNA Analysis of UCH Isozyme Genes by Real-Time PCR

SYBR Green-based real-time quantitative RT-PCR (ABI PRISM 7700 Sequence detection system, Columbia, MD) was performed [33, 35] in SYBR Green Master mix using the following primers; UCH-L1, 5′-TTCTGTTCAACAACGTGGACG-3′ and 5′-TCACTGGAAAGGGCAT TCG-3′; UCH-L3, 5′-TGAAGGTCAGACTGAGGCACC-3′ and 5′-AA TTGGAAATGGTTTCCGTCC-3′; UCH-L4, 5′-AAACAAACCATCAG CAATGCC-3′ and 5′-GACCCTGATTCAAAGTGCACC-3′; UCH-L5, 5′-TTTTCTTTTCAAGTGGCAGCC-3′ and 5′-GATAGCCTGAGTGGC ACAAGC-3′; and β-actin, 5′-CGTGCGTGACATCAAAGAGAA-3′ and 5′-CAATAGTGATGACCTGGCCGT-3′. For comparing relative UCH isozyme gene expression in isolated germ cells and Sertoli cells, the formula 2^{-ddCt} was used to calculate relative expression levels compared with spermatogonia of two-week-old mice. For comparing the expression level of UCH isozyme genes in the time course of testicular maturation, the formula 2^{-ddCt} was used to calculate relative expression levels compared with the testes of 5-day-old mice.

Western Blotting of UCH-L1 and UCH-L3 from Isolated Cells

Total protein was extracted [24] from isolated testicular cells or whole testes of 5-, 7-, 15-, 19-, 21-, 23-, 26-, and 33-day-old Balb/c mice. Control extracts were obtained from testes of *gad* and *Uchl3* knockout mice. For preparation of antibodies, we designed two specific peptides, AQHEN-FRKKQIEELKGQEVSPK (R891A, GenBank no. NP_057932, residues 57–78) and EKYEVFRTEEEEKIKSQGQDVTSS (R837A, GenBank no. NP_035800, residues 60–83) corresponding to mouse UCH-L1 and UCH-L3, respectively. Polyclonal antibodies against R891A and R837A were raised in rabbits and the IgG fraction was isolated (Tana Laboratories, L.C., Houston, TX). Each sample was adjusted to 5 μg protein/10 μl and subjected to SDS-PAGE (15% acrylamide; XV Pantera gel; DRC, Tama, Japan). After transferring the proteins to a nitrocellulose membrane and blocking with 5% skim milk, the membranes were incubated at 4°C overnight with the primary antibody to UCH-L1 (1:1000) or UCH-L3 (1:400). The membranes were then incubated with peroxidase-conjugated goat anti-rabbit IgG (H+L) (1:10 000; Pierce, Rockford, IL) for 60 min at room temperature. Immunoreactivity was visualized using the SuperSignal detection kit (Pierce) and analyzed with a ChemiImager (Alpha Innotech. San Leandro, CA).

Immunohistochemistry of UCH-L1 and UCH-L3

Tissues were fixed in vivo with 4% paraformaldehyde in phosphate-buffered saline (PBS) and embedded in paraffin, and sections (4 μm thickness) were treated with absolute methanol containing 3% H_2O_2 for 30 mir to block endogenous peroxidase activity. After blocking with 10% goa serum for 1 h at room temperature, the sections were incubated at 4°C overnight with antibodies to UCH-L1 (1:500) or UCH-L3 (1:200) dilutec in PBS containing 1% BSA. The sections were then incubated with fluorescein isothiocyanate-conjugated anti-rabbit IgG (1:200, Jackson ImmunoResearch, West Grove, PA) for 1 h at room temperature and examined by confocal laser scanning microscopy (Olympus, Tokyo, Japan)

RESULTS

Isolation of Spermatogenic Cells and Sertoli Cells

Using the c-kit antibody, we isolated an average o 17 × 10^5 type A spermatogonia from ten 2-wk-old juvenil mice and an average of 3.5 × 10^5 type A spermatogoni

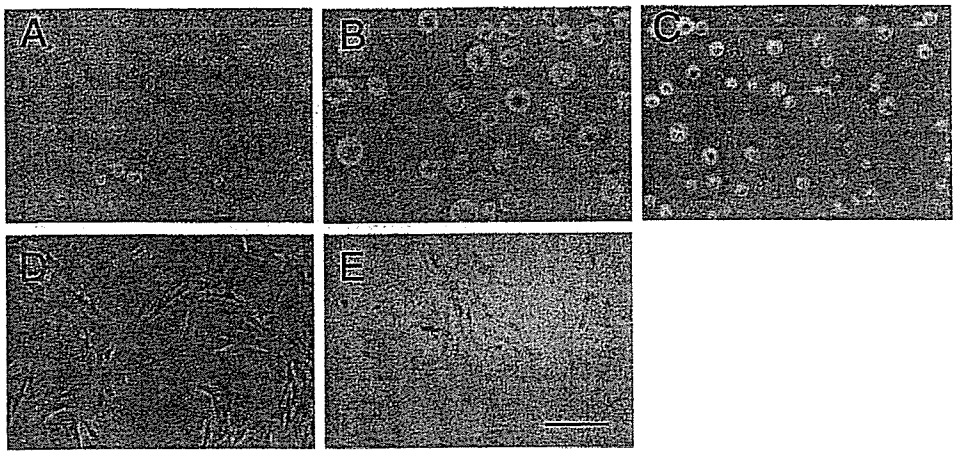

FIG. 1. Phase-contrast micrographs showing isolated germ cells and Sertoli cells from a testicular cell suspension. A) Type A spermatogonia. B) Spermatocytes. C) Spermatids. D) Sertoli cells. E) Alkaline phosphatase activity of Sertoli cell cultures. Germ cells in A–C were from testes of 8-wk-old mice. Sertoli cells in D and E were from testes of 2-wk-old mice. Scale bar = 30 μm.

from two 8-wk-old adult mice. The purity of each isolated population was <84.5% (Fig. 1A and Table 1). Using phase-contrast microscopy, we determined that these cells were 14–16 μm in diameter. Following elimination of the remaining spermatogonia using magnetic microbeads, the remaining cells were separated into two principal visible bands by centrifugation through a discontinuous Percoll gradient. Phase-contrast microscopy revealed that these two bands consisted primarily of pachytene spermatocytes and round spermatids (Fig. 1, B and C). We isolated an average of 3×10^5 spermatocytes and 200×10^5 spermatids from two 8-wk-old adult mice. We also isolated an average 20×10^5 Sertoli cells from ten 2-wk-old juvenile mice (Fig. 1D). Peritubular myoid cells were identified by alkaline phosphatase staining. Although >95% of these cells were unstained, ~5% of the Sertoli cells showed considerable alkaline phosphatase activity (Fig. 1E).

RT-PCR Analysis of Isolated Cells Expressing Specific Marker Genes

RT-PCR using extracts of isolated cells confirmed the expression of mRNAs from *c-kit*, Histone H1t, *SP-10*, and *SCF*. Each gene was expressed in only one cell type, as follows: *c-kit* in spermatogonia, the Histone H1t gene in spermatocytes, *SP-10* in spermatids, and *SCF* in Sertoli cells (Fig. 2).

Characterization of Isolated Cells by FACS

To determine the purity of isolated germ cells, we used FACS analysis to follow the differentiation-dependent acquisition of stage-specific patterns during spermatogenesis and monitored the percentage of cells with differing DNA content. The histogram in Figure 3 presents the number of cells at each fluorescence level (FL2-A). Diploid (2n DNA) cells were observed in 84.5% of the isolated spermatogonia, tetraploid (4n DNA) cells were observed in 79.6% of the isolated spermatocytes, and haploid (1n DNA) cells were observed in 85.3% of the isolated spermatids (Table 1). These results demonstrate that the majority of cells in each population exhibited the expected ploidy.

TABLE 1. The percentage of 1n, 2n, and 4n cells in isolated germ cells from a testicular cell suspension from 8-wk-old mice, as determined by FACS.[a]

Ploidy[b]	Total cells (%)[c]	Isolated germ cells (%)		
		Spermatogonia	Spermatocytes	Spermatids
1n	56.2 ± 4.2	9.4 ± 1.2	5.3 ± 1.8	85.3 ± 3.3
2n	25.2 ± 3.6	84.5 ± 2.7	9.3 ± 1.3	6.2 ± 0.9
4n	18.6 ± 3.1	12.7 ± 0.9	79.6 ± 2.5	7.7 ± 2.2

[a] Calculated after eliminating cell debris (FL2-A < 50 in Fig. 2).
[b] 1n, haploid cells (one copy of genome); 2n, diploid cells (two copies of genome); 4n, tetraploid cells (four copies of genome).
[c] Each percentage represents the mean ± SD of 4–6 measurements.

Expression of UCH Isozymes During Spermatogenesis

We characterized the expression pattern of each UCH gene in isolated testicular cell populations during spermatogenesis using SYBR Green-based real-time quantitative RT-PCR (Fig. 4). The 2^{-ddCt} values indicate the relative mRNA expression levels compared with spermatogonia from 2-wk-old mice (Sg2). The genes encoding UCH-L1 and UCH-L4 were expressed mainly in spermatogonia (Fig. 4, A and C). UCH-L1 was also expressed significantly in the Sertoli population, and UCH-L4 was expressed to a lesser degree in spermatocytes and spermatids. UCH-L3 and UCH-L5 genes were expressed primarily in the spermatid population and to a much lesser extent in spermatocytes (Fig. 4, B and D). We further examined the expression of UCH mRNAs during testicular maturation (Fig. 5A) in whole testes from 5-, 7-, 15-, 19-, 21-, 23-, 26-, and 33-

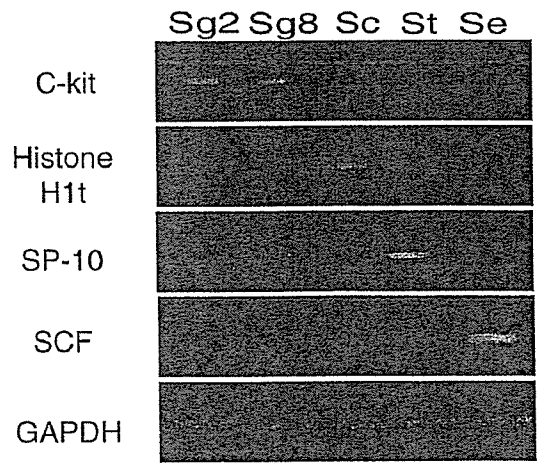

FIG. 2. Expression of c-kit, Histone H1t, SP-10, and SCF mRNAs determined by RT-PCR of extracts of isolated germ cells and Sertoli cells from a testicular cell suspension. Sg2, Spermatogonia of 2-wk-old mice; Sg8, spermatogonia from 8-wk-old mice; Sc, spermatocytes from 8-wk-old mice; St, spermatids from 8-wk-old mice; Se, Sertoli cells from 2-wk-old mice.

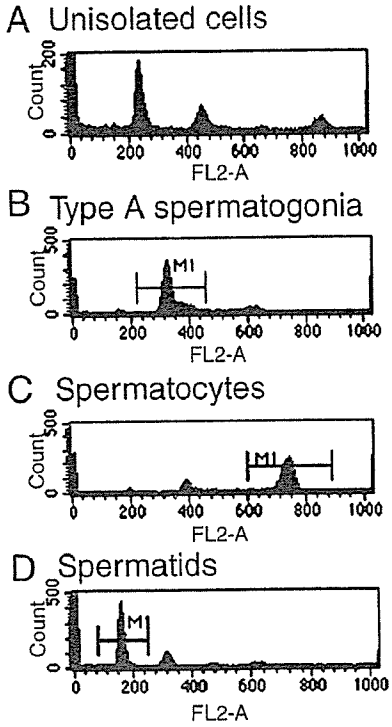

FIG. 3. FACS analysis of isolated germ cells from a testicular cell suspension obtained from 8-wk-old mice. Each window is a histogram representing the number of cells at each fluorescence level (FL2-A). A) Unisolated cells. B) Type A spermatogonia. C) Spermatocytes. D) Spermatids.

day-old mice. The UCH-L1 and UCH-L4 mRNAs were expressed similarly during development and likewise for the UCH-L3 and UCH-L5 genes. The expression of UCH-L1 mRNA appears relatively high on Postnatal Day 15. However, the percentage of spermatogonia and Sertoli cells would have become diluted by meiotic and postmeiotic germ cells after Day 15, thereby accounting for the relatively lower levels of UCH-L1 at subsequent time points. RT-PCR data suggest that UCH-L1 mRNA expression in spermatogonia and Sertoli cells increased continuously even after Postnatal Day 15 (Fig. 5B). We also analyzed the protein expression patterns of UCH-L1 and UCH-L3 in the mouse testis using peptide-specific antibodies that recognize regions in mouse UCH-L1 or UCH-L3. Western blot analysis detected UCH-L1 in spermatogonia and Sertoli cells, and UCH-L3 was detected primarily in spermatocytes and spermatids, as expected, although it was also found to a lesser extent in spermatogonia (Fig. 6A). Also, UCH-L3 expression increased in a differentiation-dependent manner during juvenile spermatogenesis (Fig. 5C). Immunohistochemistry detected homogeneous UCH-L1 expression in both spermatogonia and Sertoli cells from wild-type (Balb/c) and *Uchl3* knockout mice, whereas UCH-L3 was detected mainly in spermatocytes and round spermatids of wild-type (Balb/c) and *gad* mice (Fig. 6, B and C).

DISCUSSION

The ubiquitin pathway plays critical roles in the progression of spermatogenesis through the mitotic, meiotic, and postmeiotic phases [2, 3, 18, 36]. Because numerous proteins are regulated by ubiquitination, mutations that affect the ubiquitin pathway result in the dysregulation of multiple cellular processes and induce apoptosis during spermatogenesis [3, 37–39]. For example, mutation of HR6B, a ubiquitin-conjugating enzyme, affects both meiosis and postmeiotic germ cell development [40–43].

Ubiquitin C-terminal hydrolases catalyze the hydrolysis of C-terminal esters and amides of ubiquitin. These enzymes are believed to play a key role in processing polyubiquitin and ubiquitylated proteolytic peptides [8]. The genes for at least four UCHs, UCH-L1 and UCH-L3–5, have been identified in the mouse. Although the specificity and function of these isozymes in spermatogenesis remains elusive, each of these enzymes contains conserved residues that are critical for enzymatic activity [8–10, 44, 45]. The predominant mouse isozymes, UCH-L1 and UCH-L3, share 52% amino acid sequence identity [10, 13, 45]. However, UCH-L1 mRNA is selectively expressed in the mouse testis and nervous systems [11], whereas UCH-L3 mRNA is expressed in nearly every tissue tested, with high levels in the testis [13]. Intracellular localization of UCH-L1 was reported to be closely associated with the proliferative activity of spermatogonia and Sertoli cells [15–18]. In contrast, the expression of UCH-L3 has not been examined in the testis. To address this question, we first generated poly-

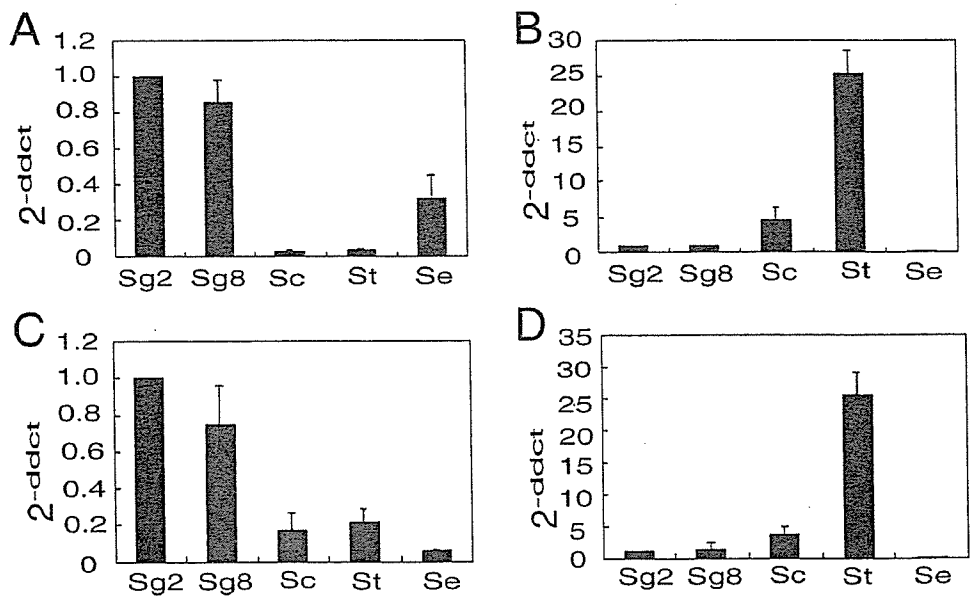

FIG. 4. Comparison of the relative UCH isozyme gene expression levels (2^{-ddCt}) in isolated germ cells and Sertoli cells using RT-PCR. The formula 2^{-ddCt} indicates the relative expression level in isolated testicular cells compared with Sg2 cells. Sg2 gene expression in each case was set to 1.0. A) *Uchl1*. B) *Uchl3*. C) *Uchl4*. D) *Uchl5*. Sg2, Spermatogonia from 2-wk-old mice; Sg8, spermatogonia from 8-wk-old mice; Sc, spermatocytes from 8-wk-old mice; St, spermatids from 8-wk-old mice; Se, Sertoli cells from 2-wk-old mice.

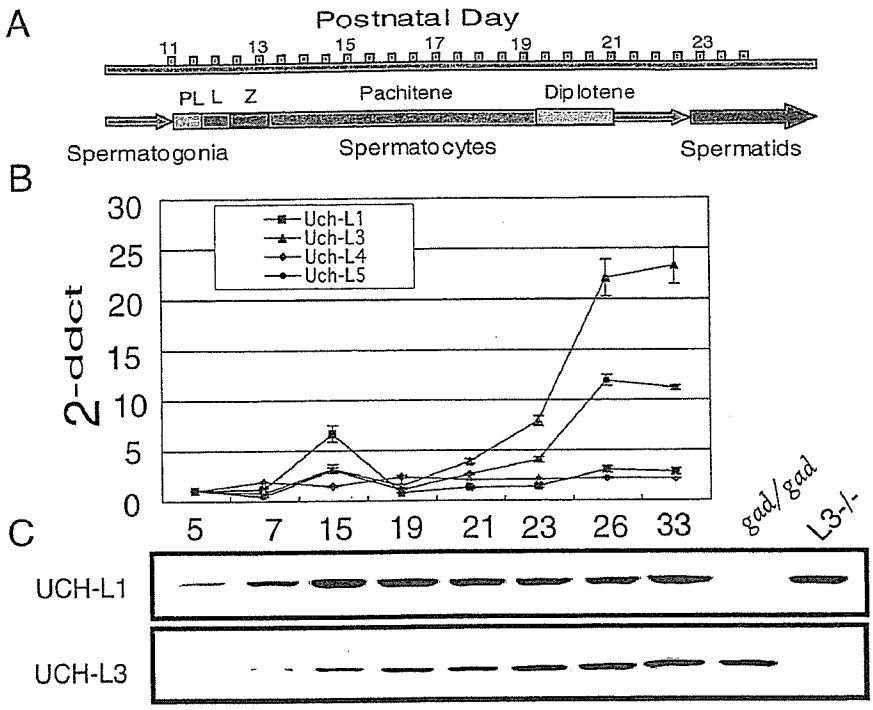

FIG. 5. Expression of UCH isozymes during testicular maturation. A) Timetable for juvenile spermatogenesis. PL, Preleptotene spermatocyte; L, leptotene spermatocyte; Z, zygotene spermatocyte. B) Comparison of the relative UCH isozyme gene expression levels (2^{-ddCt}) by SYBR Green-based real-time quantitative RT-PCR. The value for gene expression from the testes of 5-day-old mice was set to 1.0. C) Comparison of UCH-L1 and UCH-L3 expression by Western blotting. Each lane represents the testes of 5-, 7-, 15-, 19-, 21-, 23-, 26-, or 33-day-old Balb/c mice, *gad* mice, and *Uchl3* knockout mice ($L3^{-/-}$) (**B**, **C**).

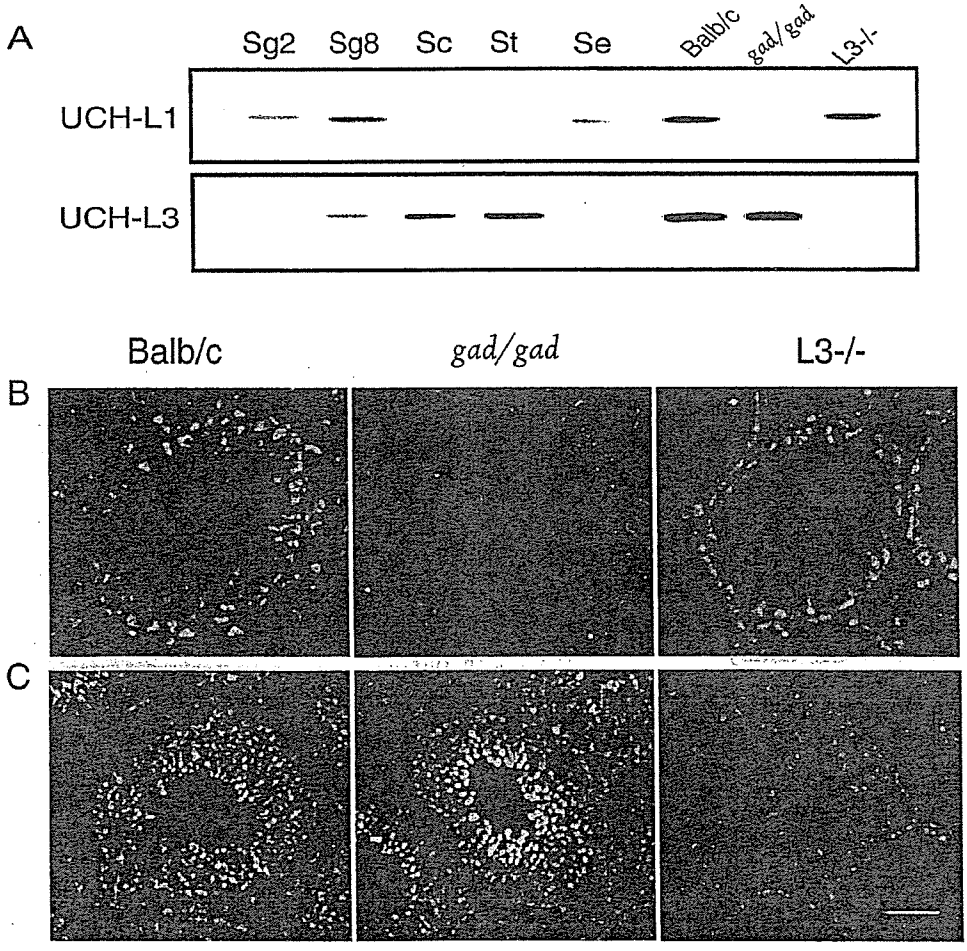

FIG. 6. Analysis of UCH-L1and UCH-L3 expression by western blotting and immunostaining. A) UCH-L1 and UCH-L3 expression in isolated germ cells and Sertoli cells. Sg2, Spermatogonia from 2-wk-old mice; Sg8, spermatogonia from 8-wk-old mice; Sc, spermatocytes from 8-wk-old mice; St, spermatids from 8-wk-old mice; Se, Sertoli cells from 2-wk-old mice. Balb/c, testis from a Balb/c mouse; *gad/gad,* testis from a *gad* mouse (*Uchl1* knockout mouse); $L3^{-/-}$, testis from a *Uchl3* knockout mouse. Immunohistochemistry of UCH-L1 (**B**) and UCH-L3 (**C**) in the testis of wild type, *gad,* and *Uchl3* knockout mouse. Stages V–VIII of seminiferous epithelium predominate in each panel as visualized by PAS staining of serial sections. Green fluorescence represents UCH-L1 (**B**) and UCH-L3 (**C**); red fluorescence represents staining of cell nuclei by propidium iodide (PI). Magnification, ×200. Scale bar = 30 μm.

clonal antibodies that specifically react with mouse UCH-L3. Using RT-PCR and western blotting, we detected high levels of UCH-L3 mRNA and protein in meiotic pachytene spermatocytes and postmeiotic spermatids during spermatogenesis (Figs. 4B and 6A). These results suggest that UCH-L1 and UCH-L3 may play distinct roles in spermatogenesis, in that UCH-L1 may function in mitotic proliferation, whereas UCH-L3 may function in the meiotic differentiation of spermatocytes into spermatids.

Around Postnatal Day 15, the higher expression of UCH-L1 mRNA suggests that UCH-L1 might have certain functions during testicular maturation. Furthermore, the increased expression of UCH-L1 after Postnatal Day 15 suggests that it might play an active role in mitotic proliferation. In addition to the *Uchl1* genes, we also analyzed transcription from two other UCH isozyme genes, *Uchl3* and *Uchl5,* in isolated testicular cells. UCH-L3 and UCH-L5 mRNAs were found in meiotic pachytene spermatocytes and postmeiotic spermatids (Fig. 4, B and D) and showed similar expression patterns during the course of testicular maturation (Fig. 5B). These results suggest that the *Uchl3* and *Uchl5* genes may have overlapping functions during spermatogenesis. The ubiquitin pathway is very active during the postmitotic phase of spermatogenesis [3, 36]. Thus, UCH-L3 may function to regulate the cell cycle and chromatin structure during the meiotic phase but may facilitate the en masse degradation of cytoplasmic proteins as well as organelle/nuclear remolding during the postmeiotic phase. The present study demonstrates for the first time that UCH-L3 is expressed mainly in meiotic spermatocytes and postmeiotic spermatids during spermatogenesis. Although UCH-L3 shares considerable sequence homology with UCH-L1, the hydrolytic activity of UCH-L3 in vitro differs substantially from that of UCH-L1. The rate of UCH-L3-mediated catalysis (K_{cat}) is more than 200 times greater than UCH-L1 using ubiquitin amide as a substrate [46]. This relatively high activity of UCH-L3 is consistent with its expression during the postmitotic phase of spermatogenesis, in that maturation from spermatocytes to spermatids may be critically dependent on the ubiquitin pathway despite the fact that *Uchl3* knockout mice exhibit normal fertility [13].

In conclusion, our results demonstrate that the expression of UCH isozymes is differentially and developmentally regulated during spermatogenesis and that UCH-L1 and UCH-L3 likely have distinct functions during different developmental phases. These results enhance our understanding of how the ubiquitin pathway is regulated by UCH isozymes during spermatogenesis. Moreover, isolation of mouse germ cells and Sertoli cells from testes may afford the opportunity to assess UCH isozyme function during spermatogenesis in vitro. UCH-L1 has been suggested to associate with monoubiquitin and thereby increase the half-life of ubiquitin in neurons [47]. In addition, a UCH-L1 ubiquityl ligase-like activity has also been proposed [46]. Further biochemical and genetic analyses of UCH family members will help elucidate the role of UCHs in the complex molecular mechanisms involved in spermatogenesis.

REFERENCES

1. Weissman AM. Themes and variations on ubiquitylation. Nat Rev Mol Cell Biol 2001; 2:169–178.
2. Baarends WM, Roest HP, Grootegoed JA. The ubiquitin system in gametogenesis. Mol Cell Endocrinol 1999; 151:5–16.
3. Baarends WM, van der Laan R, Grootegoed JA. Specific aspects of the ubiquitin system in spermatogenesis. J Endocrinol Invest 2000; 23:597–604.
4. Ciechanover A, Orian A, Schwartz AL. Ubiquitin-mediated proteolysis: biological regulation via destruction. Bioessays 2000; 22:442–451.
5. Varshavsky A. The ubiquitin system. Trends Biochem Sci 1997; 22: 383–387.
6. Wilkinson KD. Roles of ubiquitinylation in proteolysis and cellular regulation. Annu Rev Nutr 1995; 15:161–189.
7. Grimes SR, Wilkerson DC, Noss KR, Wolfe SA. Transcriptional control of the testis-specific histone H1t gene. Gene 2003; 304:13–21.
8. Wilkinson KD. Regulation of ubiquitin-dependent processes by deubiquitinating enzymes. FASEB J 1997; 11:1245–1256.
9. Mayer AN, Wilkinson KD. Detection, resolution, and nomenclature of multiple ubiquitin carboxyl-terminal esterases from bovine calf thymus. Biochemistry 1989; 28:166–172.
10. Kurihara LJ, Kikuchi T, Wada K, Tilghman SM. Loss of Uch-L1 and Uch-L3 leads to neurodegeneration, posterior paralysis and dysphagia. Hum Mol Genet 2001; 10:1963–1970.
11. Saigoh K, Wang YL, Suh JG, Yamanishi T, Sakai Y, Kiyosawa H, Harada T, Ichihara N, Wakana S, Kikuchi T, Wada K. Intragenic deletion in the gene encoding ubiquitin carboxy-terminal hydrolase in gad mice. Nat Genet 1999; 23:47–51.
12. Wilkinson KD, Deshpande S, Larsen CN. Comparisons of neuronal (PGP 9.5) and non-neuronal ubiquitin C-terminal hydrolases. Biochem Soc Trans 1992; 20:631–637.
13. Kurihara LJ, Semenova E, Levorse JM, Tilghman SM. Expression and functional analysis of Uch-L3 during mouse development. Mol Cell Biol 2000; 20:2498–2504.
14. Zhang N, Wilkinson K, Bownes M. Cloning and analysis of expression of a ubiquitin carboxyl terminal hydrolase expressed during oogenesis in *Drosophila melanogaster*. Dev Biol 1993; 157:214–223.
15. Wilson PO, Barber PC, Hamid QA, Power BF, Dhillon AP, Rode J, Day IN, Thompson RJ, Polak JM. The immunolocalization of protein gene product 9.5 using rabbit polyclonal and mouse monoclonal antibodies. Br J Exp Pathol 1988; 69:91–104.
16. Tokunaga Y, Imai S, Torii R, Maeda T. Cytoplasmic liberation of protein gene product 9.5 during the seasonal regulation of spermatogenesis in the monkey (*Macaca fuscata*). Endocrinology 1999; 140: 1875–1883.
17. Kon Y, Endoh D, Iwanaga T. Expression of protein gene product 9.5, a neuronal ubiquitin C-terminal hydrolase, and its developing change in Sertoli cells of mouse testis. Mol Reprod Dev 1999; 54:333–341.
18. Kwon J, Kikuchi T, Setsuie R, Ishii Y, Kyuwa S, Yoshikawa Y. Characterization of the testis in congenitally ubiquitin carboxy-terminal hydrolase-1 (Uch-L1) defective (gad) mice. Exp Anim 2003; 52:1–9.
19. Loveland KL, Schlatt S. Stem cell factor and c-kit in the mammalian testis: lessons originating from mother nature's gene knockouts. J Endocrinol 1997; 153:337–344.
20. Lassalle B, Ziyyat A, Testart J, Finaz C, Lefevre A. Flow cytometric method to isolate round spermatids from mouse testis. Hum Reprod 1999; 14:388–394.
21. van der Wee KS, Johnson EW, Dirami G, Dym TM, Hofmann MC. Immunomagnetic isolation and long-term culture of mouse type A spermatogonia. J Androl 2001; 22:696–704.
22. van Pelt AM, Morena AR, van Dissel-Emiliani FM, Boitani C, Gaemers IC, de Rooij DG, Stefanini M. Isolation of the synchronized A spermatogonia from adult vitamin A-deficient rat testes. Biol Reprod 1996; 55:439–444.
23. von Schonfeldt V, Krishnamurthy H, Foppiani L, Schlatt S. Magnetic cell sorting is a fast and effective method of enriching viable spermatogonia from Djungarian hamster, mouse, and marmoset monkey testes. Biol Reprod 1999; 61:582–589.
24. Kato S, Kobayashi T, Kusuda K, Nishina Y, Nishimune Y, Yomogida K, Yamamoto M, Sakagami H, Kondo H, Ohnishi M, Chida N, Yanagawa Y, Tamura S. Differentiation-dependent enhanced expression of protein phosphatase 2Cbeta in germ cells of mouse seminiferous tubules. FEBS Lett 1996; 396:293–297.
25. Anthony CT, Skinner MK. Cytochemical and biochemical characterization of testicular peritubular myoid cells. Biol Reprod 1989; 40: 811–823.
26. Scarpino S, Morena AR, Petersen C, Froysa B, Soder O, Boitani C. A rapid method of Sertoli cell isolation by DSA lectin, allowing mitotic analyses. Mol Cell Endocrinol 1998; 146:121–127.
27. Cox WG, Singer VL. A high-resolution, fluorescence-based method for localization of endogenous alkaline phosphatase activity. J Histochem Cytochem 1999; 47:1443–1456.

28. Bellve AR. Purification, culture, and fractionation of spermatogenic cells. Methods Enzymol 1993; 225:84–113.
29. Malkov M, Fisher Y, Don J. Developmental schedule of the postnatal rat testis determined by flow cytometry. Biol Reprod 1998; 59:84–92.
30. Sorrentino V, Giorgi M, Geremia R, Besmer P, Rossi P. Expression of the c-kit proto-oncogene in the murine male germ cells. Oncogene 1991; 6:149–151.
31. Kurth BE, Wright RM, Flickinger CJ, Herr JC. Stage-specific detection of mRNA for the sperm antigen SP-10 in human testes. Anat Rec 1993; 236:619–625.
32. Mauduit C, Hamamah S, Benahmed M. Stem cell factor/c-kit system in spermatogenesis. Hum Reprod Update 1999; 5:535–545.
33. Aoki K, Sun YJ, Aoki S, Wada K, Wada E. Cloning, expression, and mapping of a gene that is upregulated in adipose tissue of mice deficient in bombesin receptor subtype-3. Biochem Biophys Res Commun 2002; 290:1282–1288.
34. Janca FC, Jost LK, Evenson DP. Mouse testicular and sperm cell development characterized from birth to adulthood by dual parameter flow cytometry. Biol Reprod 1986; 34:613–623.
35. Aoki S, Su Q, Li H, Nishikawa K, Ayukawa K, Hara Y, Namikawa K, Kiryu-Seo S, Kiyama H, Wada K. Identification of an axotomy-induced glycosylated protein, AIGP1, possibly involved in cell death triggered by endoplasmic reticulum-Golgi stress. J Neurosci 2002; 22: 10751–10760.
36. Sutovsky P. Ubiquitin-dependent proteolysis in mammalian spermatogenesis, fertilization, and sperm quality control: killing three birds with one stone. Microsc Res Tech 2003; 61:88–102.
37. Wing SS. Deubiquitinating enzymes—the importance of driving in reverse along the ubiquitin-proteasome pathway. Int J Biochem Cell Biol 2003; 35:590–605.
38. Guardavaccaro D, Kudo Y, Boulaire J, Barchi M, Busino L, Donzelli M, Margottin-Goguet F, Jackson PK, Yamasaki L, Pagano M. Control of meiotic and mitotic progression by the F box protein beta-Trcp1 in vivo. Dev Cell 2003; 4:799–812.
39. van Baren MJ, van der Linde HC, Breedveld GJ, Baarends WM, Rizzu P, de Graaff E, Oostra BA, Heutink P. A double RING-H2 domain in RNF32, a gene expressed during sperm formation. Biochem Biophys Res Commun 2002; 292:58–65.
40. Escalier D, Bai XY, Silvius D, Xu PX, Xu X. Spermatid nuclear and sperm periaxonemal anomalies in the mouse Ube2b null mutant. Mol Reprod Dev 2003; 65:298–308.
41. Baarends WM, Wassenaar E, Hoogerbrugge JW, van Cappellen G, Roest HP, Vreeburg J, Ooms M, Hoeijmakers JH, Grootegoed JA. Loss of HR6B ubiquitin-conjugating activity results in damaged synaptonemal complex structure and increased crossing-over frequency during the male meiotic prophase. Mol Cell Biol 2003; 23:1151–1162.
42. Roest HP, van Klaveren J, de Wit J, van Gurp CG, Koken MH, Vermey M, van Roijen JH, Hoogerbrugge JW, Vreeburg JT, Baarends WM, Bootsma D, Grootegoed JA, Hoeijmakers JH. Inactivation of the HR6B ubiquitin-conjugating DNA repair enzyme in mice causes male sterility associated with chromatin modification. Cell 1996; 86: 799–810.
43. Escalier D. New insights into the assembly of the periaxonemal structures in mammalian spermatozoa. Biol Reprod 2003; 69:373–378.
44. Hershko A, Ciechanover A. The ubiquitin system for protein degradation. Annu Rev Biochem 1992; 61:761–807.
45. Osawa Y, Wang YL, Osaka H, Aoki S, Wada K. Cloning, expression, and mapping of a mouse gene, Uchl4, highly homologous to human and mouse Uchl3. Biochem Biophys Res Commun 2001; 283:627–633.
46. Liu Y, Fallon L, Lashuel HA, Liu Z, Lansbury PT Jr. The UCH-L1 gene encodes two opposing enzymatic activities that affect alpha-synuclein degradation and Parkinson's disease susceptibility. Cell 2002; 111:209–218.
47. Osaka H, Wang YL, Takada K, Takizawa S, Setsuie R, Li H, Sato Y, Nishikawa K, Sun YJ, Sakurai M, Harada T, Hara Y, Kimura I, Chiba S, Namikawa K, Kiyama H, Noda M, Aoki S, Wada K. Ubiquitin carboxy-terminal hydrolase L1 binds to and stabilizes monoubiquitin in neuron. Hum Mol Genet 2003; 12:1945–1958.

American Journal of Pathology, Vol. 165, No. 4, October 2004

Cell Injury, Repair, Aging and Apoptosis

Two Closely Related Ubiquitin C-Terminal Hydrolase Isozymes Function as Reciprocal Modulators of Germ Cell Apoptosis in Cryptorchid Testis

Jungkee Kwon,*† Yu-Lai Wang,* Rieko Setsuie,*‡ Satoshi Sekiguchi,† Yae Sato,*‡ Mikako Sakurai,*‡ Mami Noda,‡ Shunsuke Aoki,* Yasuhiro Yoshikawa,† and Keiji Wada*

From the Department of Degenerative Neurological Diseases, National Institute of Neuroscience, National Center of Neurology and Psychiatry, Kodaira, Tokyo; the Department of Biomedical Science,† Graduate School of Agricultural and Life Sciences, University of Tokyo, Tokyo; and the Laboratory of Pathophysiology,‡ Graduate School of Pharmaceutical Sciences, Kyushu University, Fukuoka, Japan*

The experimentally induced cryptorchid mouse model is useful for elucidating the *in vivo* molecular mechanism of germ cell apoptosis. Apoptosis, in general, is thought to be partly regulated by the ubiquitin-proteasome system. Here, we analyzed the function of two closely related members of the ubiquitin C-terminal hydrolase (UCH) family in testicular germ cell apoptosis experimentally induced by cryptorchidism. The two enzymes, UCH-L1 and UCH-L3, deubiquitinate ubiquitin-protein conjugates and control the cellular balance of ubiquitin. The testes of gracile axonal dystrophy (*gad*) mice, which lack UCH-L1, were resistant to cryptorchid stress-related injury and had reduced ubiquitin levels. The level of both anti-apoptotic (Bcl-2 family and XIAP) and prosurvival (pCREB and BDNF) proteins was significantly higher in *gad* mice after cryptorchid stress. In contrast, *Uchl3* knockout mice showed profound testicular atrophy and apoptotic germ cell loss after cryptorchid injury. Ubiquitin level was not significantly different between wild-type and *Uchl3* knockout mice, whereas the levels of Nedd8 and the apoptotic proteins p53, Bax, and caspase3 were elevated in *Uchl3* knockout mice. These results demonstrate that UCH-L1 and UCH-L3 function differentially to regulate the cellular levels of anti-apoptotic, prosurvival, and apoptotic proteins during testicular germ cell apoptosis. *(Am J Pathol 2004, 165:1367–1374)*

In the ubiquitin-proteasome system, the levels of poly- and monoubiquitin are strictly controlled by the balance of two groups of specific enzymes: ubiquitinating enzymes (E1, E2, and E3) and deubiquitinating enzymes (DUBs).[1,2] DUBs are subdivided into ubiquitin C-terminal hydrolases (UCHs) and ubiquitin-specific proteases (UBPs).[3,4] The genes for at least four UCHs, UCH-L1 and UCH-L3, UCH-L4, and UCH-L5, have been identified in mice.[5,6] Among them, UCH-L1 and UCH-L3 predominate; these isozymes have 52% amino acid identity and share significant structural similarity;[7] however, the distribution of these two isozymes is quite distinct in that UCH-L3 mRNA is expressed ubiquitously whereas UCH-L1 mRNA is selectively expressed in the testis/ovary and neuronal cells.[7–10] Despite the high-sequence homology, the *in vitro* hydrolytic activities of these two enzymes differ significantly. The activity (Kcat) of UCH-L3 is more than 200-fold higher than UCH-L1 when a fluorogenic ubiquitin substrate is used.[11] In addition to its relatively weak hydrolase activity, UCH-L1 exhibits dimerization-dependent ubiquityl ligase activity.[11] In contrast, UCH-L3 has little or no ligase activity compared with UCH-L1.[11] It was recently suggested that UCH-L1 has anti-proliferative activity in tumor cells, and that its expression is induced in response to tumor growth.[12] Furthermore, UCH-L1 associates with monoubiquitin and prolongs ubiquitin half-life in neurons.[13] Other work demonstrated that UCH-L3 binds to Nedd8 and subsequently processes its C-terminus.[14] Nedd8 is a small ubiquitin-like protein that shares with ubiquitin the ability to be conjugated to a lysine residue in a substrate protein.[15] Covalent conjugation of proteins by Nedd8 is an important form of the posttranscriptional modification and plays a critical role in many cellular processes.[16] These conju-

Supported by Grants-in-Aid for Scientific Research from the Ministry of Health, Labor, and Welfare of Japan; Grants-in-Aid for Scientific Research from the Ministry of Education, Culture, Sports, Science, and Technology of Japan; a grant from Pharmaceuticals and Medical Devices Agency of Japan; and a grant from Japan Science and Technology Agency.

Accepted for publication June 24, 2004.

Address reprint requests to Keiji Wada, Department of Degenerative Neurological Disease, National Institute of Neuroscience, National Center of Neurology and Psychiatry, Kodaira, Tokyo, 187-8502, Japan. E-mail: wada@ncnp.go.jp.

gates are regulated by a large number of deconjugating enzymes. This activity is unique to UCH-L3 because UCH-L1 is relatively weak to cleave the C terminus of Nedd8.[14–16] Collectively, these data suggest that the two mouse isozymes, UCH-L1 and UCH-L3, have distinct but overlapping functions. In addition, we recently found that *gad* mice, which lack UCH-L1 expression, show reduced retinal cell apoptosis in response to ischemia, suggesting that UCH-L1 may promote apoptosis.[17]

Our previous work focused on the possibility that UCH-L1 and UCH-L3 exhibit functional diversity during spermatogenesis. We showed that both UCH-L1 and UCH-L3 are strongly but reciprocally expressed in the testis during spermatogenesis,[18] suggesting that each isozyme may have a distinct function in the testis. To elucidate the pathophysiological roles of these two isozymes in the testis, our present work examines the extent of heat-induced stress using experimentally induced cryptorchidism in *Uchl3* knockout[7] and *gad* mice.[8] Normally, the testes are maintained in the scrotum at a temperature lower than that of the abdomen. Exposure of a testis to higher body temperature via experimentally induced cryptorchidism results in rapid degeneration of testicular germ cells.[19–22] Recent studies show that testicular germ cell degeneration in cryptorchid testes occurs via apoptosis, and that protein and lipid oxidation, along with p53 promote germ cell death.[23–25] The ubiquitin-proteasome system is required for the subsequent degradation of the damaged testicular germ cells.[26–28] Here, we show that both UCH-L1 and UCH-L3 have reciprocal functions in testicular germ cells during cryptorchid-induced apoptosis. Our data show that the absence of UCH-L1 causes resistance to cryptorchid-induced testicular germ cell apoptosis, and that the knockout of UCH-L3 promotes germ cell apoptosis after cryptorchid injury.

Materials and Methods

Animals

We used 8-week-old *Uchl3* knockout (C57BL/6J)[7,18] and *gad*[8,18,29] (CBA/RFM) male mice. *Uchl3* knockout mice were generated by the standard method using homologously recombinant ES cells, and the knockout line was back-crossed several times to C57BL/6J mice.[7] The *gad* mouse is an autosomal recessive mutant that was obtained by crossing CBA and RFM mice.[8] The *gad* line was maintained by intercrossing for more than 20 generations.[8,29] Both strains were maintained at our institute. Animal care and handling were in accordance with institutional regulations for animal care and were approved by the Animal Investigation Committee of the National Institute of Neuroscience, National Center of Neurology and Psychiatry, Tokyo, Japan.

Unilateral Experimental Cryptorchidism

Unilateral cryptorchidism was experimentally induced under pentobarbital anesthesia (Abbott Laboratories, North Chicago, IL).[20,22] Briefly, a midline abdominal incision was made, and the left testis was displaced from scrotum and fixed to the upper abdominal wall. The right testis remained in the scrotum as an intact control within the same animal. At 0, 4, 7, and 14 days after the operation, four control and four cryptorchid testes were harvested to determine testis weight.

Histological and Immunohistochemical Assessment of Testes

Testes were embedded in paraffin wax after fixation in 4% paraformaldehyde, sectioned at 4-μm thickness, and stained with hematoxylin and eosin.[29] Light microscopy was used for routine observations. For immunohistochemical staining, the sections were incubated with 10% goat serum for 1 hour at room temperature, followed by incubation overnight at 4°C with a rabbit polyclonal antibody against ubiquitin (1:500; DakoCytomation, Glostrup, Denmark) or Nedd8 (1:500; Alexis Biochemicals, San Diego, CA) diluted in phosphate-buffered saline (PBS) containing 1% bovine serum albumin. Sections were then incubated with fluorescein isothiocyanate-conjugated goat anti-rabbit IgG (1:200; Jackson ImmunoResearch, West Grove, PA) for 1 hour at room temperature and examined by confocal laser-scanning microscopy (Olympus, Tokyo, Japan).

Apoptotic cells in testicular tissues were identified by terminal deoxynucleotidyl transferase (TdT)-mediated nick-end labeling (TUNEL) using the DeadEnd Fluorimetric TUNEL system kit (Promega, Madison, WI) and the anti-PARP p85 fragment pAb (Promega) according to the manufacturer's instructions.

Quantitative Analysis of Apoptotic Germ Cells

The number of apoptotic cells was determined by counting the positively stained nuclei in 30 circular seminiferous tubule cross-sections per testis section.[23,29] The proportion of seminiferous tubules containing apoptotic germ cells was calculated by dividing the number of seminiferous tubules containing apoptotic cells by the total number of seminiferous tubules. The incidence of apoptotic cells per apoptotic cell-containing seminiferous tubule was categorized into three groups, defined as 1 to 5, 6 to 10, and >11 positive cells.

Western Blotting

Western blots were performed as previously reported.[8,18,29] Total protein (5 μg/lane) was subjected to sodium dodecyl sulfate-polyacrylamide gel electrophoresis using 15% gels (Perfect NT Gel; DRC, Japan). Proteins were electrophoretically transferred to polyvinylidene difluoride membranes (Bio-Rad, Hercules, CA) and blocked with 5% nonfat milk in TBS-T [50 mmol/L Tris base, pH 7.5, 150 mmol/L NaCl, 0.1% (w/v) Tween-20]. The membranes were incubated individually with one or more primary antibodies to UCH-L1 and UCH-L3 (1:1000; peptide antibodies[18]), Bcl-2, Bcl-xL, Bax, p53, and caspase-3, (1:1000; all from Cell Signaling Technology, Beverly, MA), phosphorylated cyclic AMP response element-binding protein (pCREB, 1:500; Upstate Biotech-

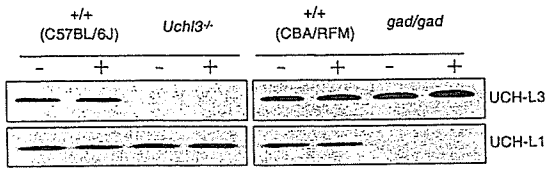

Figure 1. Western blotting analyses of both UCH-L3 and UCH-L1 in the testes of *gad* and *Uchl3* knockout mice, respectively, on day 4 after cryptorchid injury. Scrotal and cryptorchid testes did not differ significantly with respect to protein expression (−, scrotal testes; +, cryptorchid testes).

nology, Waltham, MA), brain-derived neurotrophic factor (BDNF, 1:500; Santa Cruz Biotechnology, Santa Cruz, CA), XIAP (1:500; Transduction Laboratories, Franklin Lakes, NJ), polyubiquitin (1:1000, clone FK-2; Medical & Biological Laboratories, Nagoya, Japan), monoubiquitin (1:1000, u5379; Sigma-Aldrich, St. Louis, MO), and Nedd8 (1:1000; Alexis Biochemicals, San Diego, CA). Blots were further incubated with peroxidase-conjugated goat anti-mouse IgG or goat anti-rabbit IgG (1:5000; Pierce, Rockford, IL) for 1 hour at room temperature. Immunoreactions were visualized using the SuperSignal West Dura extended duration substrate (Pierce) and analyzed with a ChemiImager (Alpha Innotech, San Leandro, CA). Each protein level was relatively quantificated after analysis with a ChemiImager using AlphaEase software.

Statistical Analysis

The mean and SD were calculated for all data (presented as mean ± SD). One-way analysis of variance was used for all statistical analyses.

Results

Level of Two UCH Isozymes in Scrotal and Cryptorchid Testes from Uchl3 Knockout and Gad Mice

We first confirmed the lack of UCH-L3 protein in the testes from *Uchl3* knockout mice by Western blotting (Figure 1). Similarly, we did not detect UCH-L1 protein in the testes of *gad* mice (Figure 1), as we previously observed.[13] Thus, in a biochemical sense, *gad* mice are analogous to *Uchl1*-null mice.[8,13] Compensatory level of UCH-L3 and UCH-L1 in *gad* and *Uchl3* knockout mice, respectively, was not observed (Figure 1; compare UCH-L3/UCH-L1 level with that of wild-type control mice). Experimental cryptorchidism did not affect UCH-L3 level in *gad* or wild-type control mice. Similarly, cryptorchidism did not affect UCH-L1 level in *Uchl3* knockout and wild-type control mice (Figure 1). Quantitative reverse transcriptase-polymerase chain reaction analysis showed that transcription from the *Uchl3* and *Uchl1* in both scrotal and cryptorchid testes from *gad* and *Uchl3* knockout mice was not significantly different from that measured in the corresponding wild-type control mice (data not shown). These results suggest that the level of UCH-L3 is regulated independently of UCH-L1 in the mouse testis, and that cryptorchid injury does not affect the level of either protein.

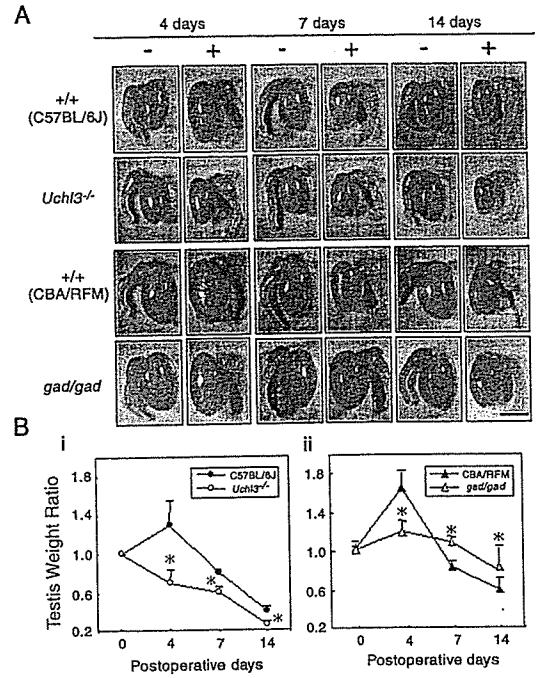

Figure 2. Comparison of testicular sizes and weights after experimental cryptorchidism. **A:** Gross images of changes in testicular size throughout time in two wild-type (C57BL/6J and CBA/RFM), *Uchl3* knockout, and *gad* mice (−, scrotal testes; +, cryptorchid testes). **B:** Ratio of cryptorchid to scrotal testis weight on days 0, 4, 7, and 14 after injury. i: Throughout time, the ratio for *Uchl3* knockout mice (**open circles**) differed significantly compared with wild-type mice (**filled circles**). ii: The ratio for *gad* mice (**open triangles**) did not differ significantly throughout time compared with wild-type mice (**closed triangles**). ($n = 4$; *, $P < 0.05$). Scale bar, 5 mm. Original magnifications, ×40.

Changes in Testicular Weight and Structure in Cryptorchid Uchl3 Knockout and Gad Mice

Unilateral cryptorchidism was surgically induced in *Uchl3* knockout and *gad* mice, and testes were evaluated on days 0, 4, 7, and 14 after the operation (Figure 2). Nonoperated (scrotal) testes served as controls for the evaluation of testicular weight and histochemistry. Cryptorchid testes from *Uchl3* knockout mice appeared smaller than the nonoperated controls at each time point, whereas the size of the cryptorchid testes from *gad* mice was similar to the controls (Figure 2A). Figure 2B shows the time course of the ratio of testicular weight of cryptorchid testes to scrotal testes. In wild-type mice (C57BL/6J and CBA/RFM), the ratio transiently increased 4 days after cryptorchid injury, most likely a consequence of inflammation-induced fluid accumulation[22,23] and biochemical changes observed. The ratio for these mice subsequently decreased below 1.0 by day 7. The ratio remained ~1.0 in *gad* mice (range,1.15 ~ 0.85), whereas it decreased significantly in *Uchl3* knockout mice compared with wild-type mice (Figure 2B). These results demonstrate that testes from *Uchl3* knockout and *gad* mice differ in their response to experimental cryptorchidism.

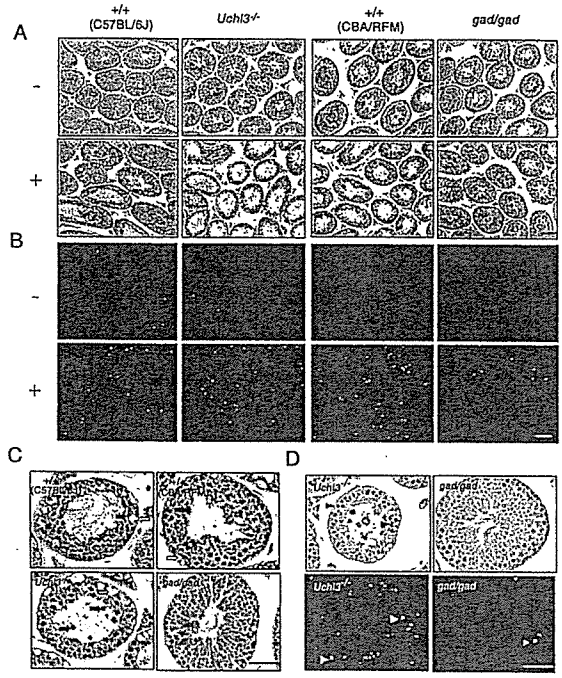

Figure 3. Histology and TUNEL staining of testicular cross sections after experimental cryptorchidism. **A:** Morphological analysis of seminiferous tubules on day 7 after cryptorchid injury. Note the germ cell loss and atrophy in cryptorchid testes compared with uninjured controls. (−, scrotal testes; +, cryptorchid testes). **B:** TUNEL staining of testicular cross-sections on day 7 after cryptorchid injury. Green fluorescence, TUNEL-positive cells; red fluorescence, nuclei stained with propidium iodide. **C:** Magnified cryptorchid testes sections. Pyknotic bodies (**filled arrows**) and Sertoli cell vacuolization (**open arrows**) were evident in cryptorchid testes of *Uchl3* knockout and the two wild-type (C57BL/6J and CBA/RFM) mice on day 7 after injury. **D:** PARP analysis to detect apoptotic germ cells in cryptorchid testes of *Uchl3* knockout and *gad* mice on day 7 after injury. The detection of apoptotic germ cells (**arrowheads, top**) by PARP analysis was consistent with that of apoptotic germ cells (**arrowheads, bottom**) by TUNEL analysis. Scale bar, 50 μm. Original magnifications: **A** and **B** ×100; **C** and **D** ×200.

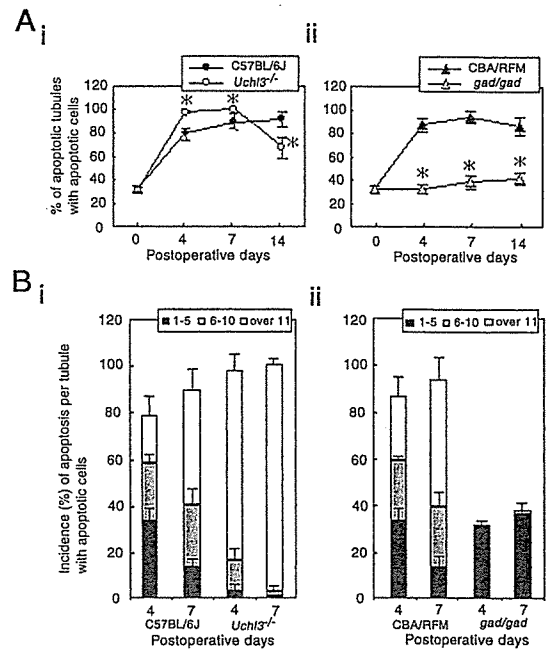

Figure 4. Quantitation of testicular germ cell apoptosis in testes after experimental cryptorchidism. **A:** The percentage of seminiferous tubules containing apoptotic germ cells in cryptorchid testes on days 0, 4, 7, and 14 after injury. **i:** The increase in the percentage of tubules containing apoptotic cells in the cryptorchid testes of *Uchl3* knockout mice is statistically significant compared with wild-type mice on days 4, 7, and 14. Each value represents the mean ± SD; *, $P < 0.05$. **ii:** The percentage of apoptotic tubules in cryptorchid testes of *gad* mice is significantly different on days 4, 7, and 14 after injury. Each value represents the mean ± SD; *, $P < 0.01$. **B:** Incidence of apoptosis per seminiferous tubule with apoptotic germ cells on days 4 and 7 after injury. The incidence of seminiferous tubules containing >11 apoptotic germ cells is significantly increased ($P < 0.05$) in cryptorchid testes of *Uchl3* knockout mice compared with wild-type mice. **i:** Comparison with *Uchl3* knockout mice. **ii:** Comparison with *gad* mice. Each value represents the mean ± SD.

Testicular Germ Cell Apoptosis in Cryptorchid Uchl3 Knockout and Gad Mice

To explore the mechanism underlying the observed differences between *Uchl3* knockout and *gad* cryptorchid testes, we prepared histological cross-sections on day 7 after testicular injury (Figure 3, A and C). The presence of nuclear pyknosis, multinucleated giant cells, and Sertoli cell vacuolization with germ cell loss in the germinal epithelium is indicative of cryptorchid testes.[22,23] These hallmarks of testicular injury were the most remarkable characteristics of cryptorchid testes from *Uchl3* knockout mice, demonstrating profound testicular atrophy and germ cell loss compared with wild-type mice (Figure 3, A and C). In contrast, no nuclear pyknosis, cellular shrinkage, or germ cell loss was observed in cryptorchid testes from *gad* mice. Spermatocytes and early spermatids comprised the majority of affected cell types in cryptorchid testes (Figure 3, A and C).

Germ cell apoptosis was further examined by TUNEL and PARP assays in tissue sections from postoperative day 7 mice (Figure 3, B and D). All but the *gad* cryptorchid testes showed a time-dependent increase in germ cell apoptosis during experimental cryptorchidism; germ cell apoptosis was always found in tubules that had germ cell loss on days 4, 7, and 14 (Figure 3, B and D, and Figure 4). Compared to wild-type mice, the cryptorchid testes of *Uchl3* knockout mice showed a marked increase in apoptotic germ cells in response to testicular injury, whereas *gad* mice lacked cryptorchid-induced germ cell apoptosis (Figure 3B and Figure 4). By postoperative days 4 and 7, the percentage of seminiferous tubules containing apoptotic germ cells increased with statistical significance ($n = 4$) ($P < 0.05$) in cryptorchid testes of *Uchl3* knockout mice as compared with wild-type mice (Figure 4A). In addition, cryptorchid testes of *Uchl3* knockout mice showed a high incidence of seminiferous tubules containing >11 apoptotic germ cells on days 4 and 7 days as compared with wild-type mice (Figure 4B); however, germ cell apoptosis did not increase in cryptorchid testes of *gad* mice during postoperative days 4 to 14 ($P < 0.01$) (Figure 4, A and B).

Cellular Mono- and Polyubiquitin Level in Cryptorchid Uchl3 Knockout and Gad Mice

Ubiquitin is required for energy-dependent degradation of structurally altered proteins.[26] We previously reported that UCH-L1 binds ubiquitin and stabilizes ubiquitin turnover in neurons, and that the level of monoubiquitin is decreased in *gad* mice.[13] In a model of ischemic insult in the retina, ubiquitin induction was unexpectedly lower and ischemic

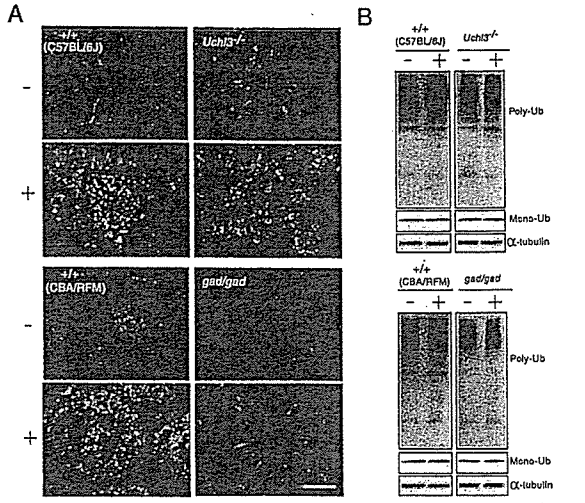

Figure 5. Immunohistochemical and Western blotting analyses of mono- and polyubiquitin in testes on day 7 after experimental cryptorchidism. **A:** Ubiquitin induction was not different between cryptorchid testes from *Uchl3* knockout and wild-type mice, whereas cryptorchid-induced ubiquitin induction in *gad* mice was reduced. Green fluorescence, ubiquitin-positive cells; red fluorescence, nuclei stained with propidium iodide. **B:** Polyubiquitin level in *Uchl3* knockout mice and the two wild-type (C57BL/6J and CBA/RFM) mice substantially increased after injury, whereas that in *gad* mice did not change significantly. Monoubiquitin level did not change after injury. Representative images from four independent experiments are shown (−, scrotal testes; +, cryptorchid testes). Scale bar, 50 μm. Original magnifications, ×200.

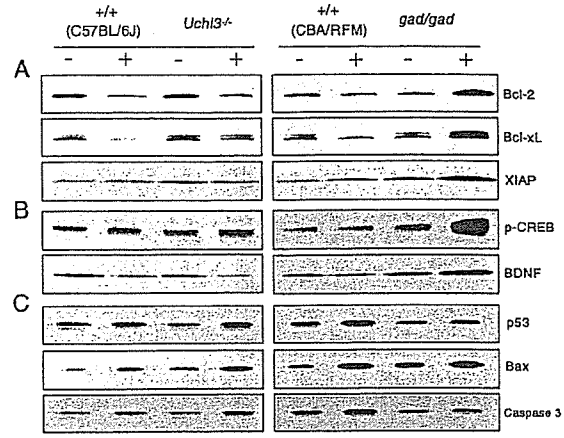

Figure 6. Western blotting analysis of anti-apoptotic, prosurvival, and apoptotic proteins in testes after experimental cryptorchidism. Total protein (5 μg per lane) was prepared from scrotal and cryptorchid testes on day 4 after cryptorchid injury. The expression levels of anti-apoptotic (**A**), prosurvival (**B**), and apoptotic (**C**) proteins in the cryptorchid testes of *Uchl3* knockout, *gad*, and the two wild-type (C57BL/6J and CBA/RFM) mice were significantly different compared with control mice. Representative images from four independent experiments are shown (−, scrotal testes; +, cryptorchid testes).

damage was weaker in the retina of *gad* mice (compared with wild-type mice) after ischemic insult.[17] To determine whether the increase in germ cell apoptosis in cryptorchid testes is associated with ubiquitin induction, we performed immunohistochemical analysis of testes from postoperative day 7 mice. Ubiquitin immunoreactivity increased substantially in cryptorchid testes from *Uchl3* knockout mice and the two wild-type mice, whereas those from *gad* mice showed only minor ubiquitin induction (Figure 5A). The scrotal testes of *Uchl3* knockout and *gad* mice did not show significant differences in ubiquitin induction compared with corresponding controls (Figure 5A). Interestingly, most of the increased ubiquitin induction was detected in spermatocytes and spermatids, consistent with the data on germ cell apoptosis after cryptorchid injury (Figure 3D and Figure 5A). Cryptorchid-induced polyubiquitin levels in the testes from *Uchl3* knockout and the two wild-type mice also increased substantially after injury, whereas the cryptorchid testes of *gad* mice showed no significant difference compared with scrotal testes (Figure 5B); however, the expression levels of monoubiquitin did not change significantly in any of the mice after cryptorchid injury.

Level of Anti-Apoptotic and Apoptotic Proteins in Cryptorchid Uchl3 Knockout and Gad Mice

We previously showed that anti-apoptotic proteins such as Bcl-2 and prosurvival proteins including phosphorylated cyclic AMP response element-binding protein (pCREB) are up-regulated in degenerated retina of *gad* mice.[17] These proteins are degraded by ubiquitination-mediated proteolysis.[30] We examined the expression of the Bcl-2 family proteins, XIAP, pCREB, and caspases to determine their role in testicular germ cell apoptosis after experimental cryptorchidism 4 days after injury in *Uchl3* knockout and *gad* mice. The level of anti-apoptotic proteins such as Bcl-2, Bcl-xL, and XIAP was up-regulated (323.8 ± 57.5, 262.3 ± 22.1, and 209.9 ± 11.7, respectively, as compared with wild type, 100) in the cryptorchid testes of *gad* mice compared with wild-type mice (Figure 6A). Additionally, pCREB, which is normally degraded in a ubiquitination-mediated manner,[30] was apparently highly up-regulated (259.0 ± 22.6, as compared with wild type, 100) in the cryptorchid testes of *gad* mice (Figure 6B). It has been demonstrated that pCREB activates genes that up-regulate trophic factors including BDNF.[31,32] Consistent with pCREB up-regulation, BDNF level also increased (203.0 ± 19.6, as compared with wild type, 100) in cryptorchid testes of *gad* mice (Figure 6B). Level was variable for anti-apoptotic, prosurvival, and apoptotic proteins in the cryptorchid testes of *Uchl3* knockout mice. The level of pCREB, p53, Bax, and caspase3 was slightly increased (169.9 ± 15.2, 152.6 ± 12.9, and 157.3 ± 14.0, respectively, as compared with scrotal testes, 100) in cryptorchid testes of *Uchl3* knockout mice compared with scrotal testes (Figure 6, B and C). Wild-type control mice had a similar expression level pattern except for pCREB. Because p53 acts as an upstream activator of Bax expression,[33] the observed Bax up-regulation after cryptorchid injury was consistent with the elevated p53 level in *Uchl3* knockout and wild-type control mice (Figure 6C). In contrast, BDNF was down-regulated (74.3 ± 7.7 as compared with wild type, 100) in cryptorchid testes of *Uchl3* knockout mice (Figure 6B). The down-regulation of BDNF combined with the up-regulation of pCREB suggests that BDNF might be regulated by another pathway that involves UCH-L3 but not pCREB.[34] Compared with scrotal testes, the expression of anti-apoptotic proteins decreased or was unchanged in cryptorchid testes of *Uchl3* knockout mice (Figure 6A).

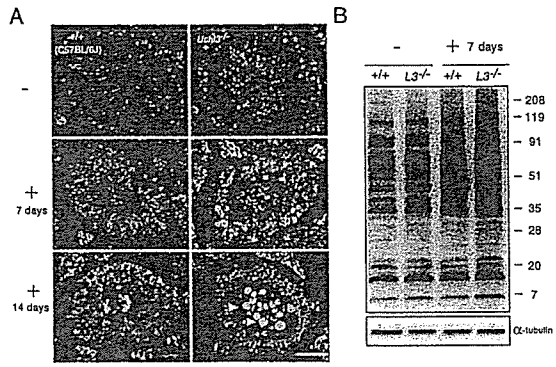

Figure 7. Immunohistochemical and Western blotting analyses of Nedd8 in testes from *Uchl3* knockout mice on days 7 and 14 after experimental cryptorchidism. **A:** Nedd8 induction in *Uchl3* knockout mice increased in both scrotal and cryptorchid testes. The shedding germ cells (**arrowheads**) in the cryptorchid testes of *Uchl3* knockout mice showed strong Nedd8 induction (−, scrotal testes; +7 days and + 4 days, cryptorchid testes). Green fluorescence, Nedd8-positive cells; red fluorescence, nuclei stained with propidium iodide. **B:** On day 7, the expression levels of Nedd8-conjugated proteins in *Uchl3* knockout mice were higher than in wild-type mice. Representative images of four independent experiments are shown. Scale bar, 50 μm. Original magnifications, ×200.

Nedd8 Level in Cryptorchid Uchl3 Knockout Mice

The varied expression levels of ubiquitin, anti-apoptotic, and apoptotic proteins in cryptorchid testes did not adequately explain the relatively exacerbated testicular atrophy and germ cell loss in *Uchl3* knockout mice compared with wild-type mice. We explored the underlying mechanism of this observation using the fact that UCH-L3 cleaves Nedd8.[14,16] We tested whether any change in Nedd8 expression correlated with greater testicular atrophy and germ cell loss in *Uchl3* knockout mice. Nedd8 immunoreactivity was highly detected in scrotal and cryptorchid testes from *Uchl3* knockout mice compared with wild-type mice (Figure 7A). The increased Nedd8 induction was mainly observed in spermatocytes and spermatids, and its expression pattern was similar to that of UCH-L3 during spermatogenesis.[18] These results suggest that Nedd8 may interact closely with UCH-L3 during testicular atrophy and germ cell loss. The cryptorchid testes of *Uchl3* knockout mice showed time-dependent and rapid Nedd8 induction compared with wild-type mice throughout the period 7 to 14 days after injury (Figure 7A). Moreover, the cryptorchid testes of *Uchl3* knockout mice showed strong Nedd8 induction in luminal shedding germ cells on day 14. An immunoblot of scrotal and cryptorchid testes proteins on day 7 confirmed the higher expression levels of Nedd8-conjugated proteins in *Uchl3* knockout mice as compared with wild-type mice (Figure 7B).

Discussion

During spermatogenesis, apoptosis controls germ cell numbers and eliminates defective germ cells to facilitate testicular homeostasis.[35–37] Recent studies indicate that ubiquitination targets proteins for degradation and modulates the turnover of various classes of short-lived signaling proteins.[28,38] Germ cell apoptosis after cryptorchid stress involves genes for various factors, such as Bcl-2 family proteins, p53, and caspases;[39–44] however, the impact of the ubiquitin system on the regulatory mechanisms of germ cell apoptosis is not fully understood. In a previous study, we used *gad* mice, which lack UCH-L1 expression, to show that neural cell apoptosis is suppressed after ischemic retinal injury *in vivo*.[17] These results suggest that UCH-L1 is involved in apoptosis-inducing pathways after stress. UCH-L1 and UCH-L3 are highly similar in sequence; however, UCH-L3 is expressed ubiquitously,[7] whereas UCH-L1 is selectively expressed in neurons and testes/ovaries.[8,9] We recently demonstrated that the expression of these UCH isozymes is differentially and developmentally regulated during spermatogenesis, and that UCH-L1 and UCH-L3 likely have distinct functions during different developmental phases.[18]

To understand the pathophysiological roles of UCH-L1 and UCH-L3 *in vivo*, two mutant mice, *Uchl3* knockout and *gad* mice, were examined after cryptorchid injury. The cryptorchid testes of the two mutant mice had fundamental differences after injury, in that testes of *Uchl3* knockout mice showed profound apoptosis-mediated germ cell loss, whereas *gad* mice were relatively resistant to injury (Figures 3 and 4). In addition, cryptorchid testes of *Uchl3* knockout mice showed greater testicular atrophy and germ cell loss than wild-type mice.

There are several proposed mechanisms for germ cell loss after experimental cryptorchidism.[21–23,45] The tumor suppressor protein, p53, is highly expressed in the testis and regulates both cell proliferation and apoptosis.[23,28,37] A role for p53 in experimental cryptorchidism has been demonstrated convincingly. The higher temperature of the testis caused by cryptorchidism induces p53-mediated apoptosis in the testis, and p53 overexpression results in increased germ cell apoptosis and decreased spermatozoa production.[23,46] In addition to p53, the Bcl-2 family and IAP (inhibitor of apoptosis protein) family are other major classes of intracellular apoptosis regulators.[47,48] The Bcl-2 family can be divided into anti-apoptotic members, such as Bcl-2, Bcl-xL, and Bcl-w, and proapoptotic members, such as Bax and Bak.[49] It has been suggested that the ratio of proapoptotic to anti-apoptotic Bcl-2 family members is important in determining whether a cell will undergo apoptosis.[49] A major function of the Bcl-2 family members appears to be the regulation of mitochondrial events, such as the release of proapoptotic factors.[50] The IAP family inhibits apoptosis primarily by inactivating and degrading proapoptotic proteins.[51] XIAP, a member of IAP family, can bind to and inhibit the proteinase activity of cellular caspase-3 and caspase-9, and thereby block the apoptotic process.[44,52,53]

With regard to cryptorchid injury, the balance between the expression of apoptosis-inducing and apoptosis-protecting proteins constitutes one possible mechanism underlying the observed germ cell apoptosis and protection from apoptosis in *Uchl3* knockout and *gad* mice, respectively. In *gad* mice, cryptorchid injury caused a large increase in the anti-apoptotic proteins Bcl-2, Bcl-xL, and XIAP, consistent with our previous report using retina.[17]

In addition, the expression levels of the prosurvival proteins pCREB and BDNF also increased in *gad* mice. Consistent with these results, caspase-3 expression was suppressed in *gad* mice. Cryptorchid testes of *Uchl3* knockout mice showed slightly increased expression of the apoptotic proteins p53, Bax, and caspase-3 after injury, although similar increases were also observed in wild-type control mice. In total, these results suggest that UCH-L1 plays a role in balancing the expression of apoptosis-inducing and apoptosis-protecting proteins. In contrast, UCH-L3 seems to resist germ cell apoptosis after cryptorchid injury.

Recent studies demonstrate that many molecules in the cellular apoptosis machinery, such as p53,[39,41] Bcl-2 family,[42,43,54] XIAP,[52] and caspase[44] members, are targets for ubiquitination.[28] This suggests that ubiquitination is one of the major mechanisms by which apoptotic cell death is regulated. UCH-L1 has been suggested to associate with monoubiquitin,[13] and the monoubiquitin pool is reduced in *gad* mice relative to wild-type mice. Protection from cryptorchid injury was reported in testes of mice expressing a mutant K48R ubiquitin,[22] suggesting that ubiquitin plays a critical role in processing or modulating testicular insults. Normally, damaged proteins are polyubiquitinated and degraded via the ubiquitin-proteasome system; however, if damaged proteins are not degraded as easily when monoubiquitin is either depleted or mutated, then germ cell death could be delayed.[17,22] Our results with the *gad* mouse suggest that ubiquitin induction plays a critical role in regulating cell death during cryptorchid injury-mediated germ cell apoptosis.

Uchl3 knockout mice exhibit severe retinal degeneration, suggesting that the UCH-L3-mediated ubiquitin pathway is involved in retinal homeostasis.[55] In the cryptorchid testes of *Uchl3* knockout mice, however, the profound testicular weight reduction and germ cell apoptosis after injury cannot be explained by ubiquitin induction alone. Our present results show that *Uchl3* knockout and wild-type mice have similar ubiquitin expression level in the testes, suggesting that UCH-L3 has another nonhydrolase activity in the ubiquitin-proteasome system. UCH-L3 also binds and cleaves the C-terminus of the ubiquitin-like protein, Nedd8.[14,56] This activity is unique to UCH-L3 because UCH-L1 does not cleave Nedd8. Thus, UCH-L3 appears to have dual affinities for ubiquitin and Nedd8. Our present results show that Nedd8 is strongly induced in scrotal testes of *Uchl3* knockout mice compared with those of wild-type mice (Figure 7). Cryptorchid testes of both *Uchl3* knockout and wild-type mice showed Nedd8 induction after injury, although the induction was higher in *Uchl3* knockout mice. These observations suggest that UCH-L3 may function as a deneddylating enzyme[16] *in vivo*, although further studies are necessary to clarify whether UCH-L3 interacts with Nedd8 during spermatogenesis.

In the present study, we demonstrate apparent reciprocal functions for the two deubiquitinating enzymes, UCH-L1 and UCH-L3, with respect to mediating injury after experimental cryptorchidism (Figure 8). Our results advance our understanding of the role of the ubiquitin-proteasome system in regulating apoptosis, and provide a unique opportunity for effective therapeutic intervention.

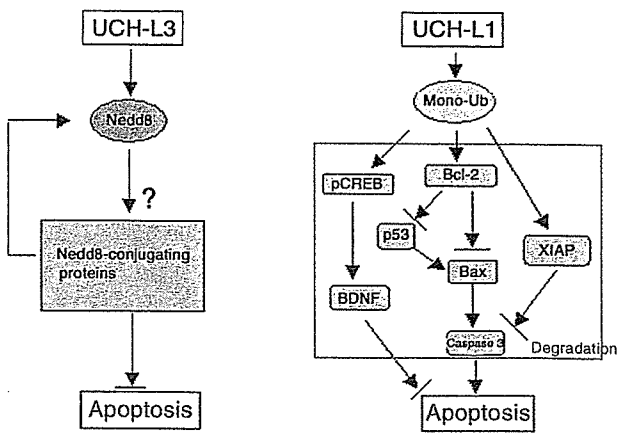

Figure 8. Differential function of the two UCH isozymes in response to experimental cryptorchidism. UCH-L3 has specificity for Nedd8. Cryptorchid injury results in protein damage and the accumulation of Nedd8-conjugated proteins. The accumulation of Nedd8-conjugated proteins in *Uchl3* knockout mice may contribute to profound germ cell loss via apoptosis. Hence, UCH-L3 might function as an anti-apoptotic regulator. UCH-L1 is involved in the maintenance of monoubiquitin levels. A deficiency in monoubiquitin results in delayed polyubiquitination and the accumulation of short-lived proteins after cryptorchid injury. Hence, UCH-L1 may function as a regulator of apoptosis.

Acknowledgments

We thank Dr. S.M. Tilghman for providing *Uchl3* knockout mice, H. Kikuchi for technical assistance with tissue sections, and M. Shikama for the care and breeding of animals.

References

1. Weissman AM: Themes and variations on ubiquitylation. Nat Rev Mol Cell Biol 2001, 2:169–178
2. Ciechanover A: The ubiquitin-proteasome pathway: on protein death and cell life. EMBO J 1998, 17:7151–7160
3. Pickart CM, Rose IA: Ubiquitin carboxyl-terminal hydrolase acts on ubiquitin carboxyl-terminal amides. J Biol Chem 1985, 260:7903–7910
4. Baker RT, Tobias JW, Varshavsky A: Ubiquitin-specific proteases of Saccharomyces cerevisiae. Cloning of UBP2 and UBP3, and functional analysis of the UBP gene family. J Biol Chem 1992, 267:23364–23375
5. Osawa Y, Wang YL, Osaka H, Aoki S, Wada K: Cloning, expression, and mapping of a mouse gene, Uchl4, highly homologous to human and mouse Uchl3. Biochem Biophys Res Commun 2001, 283:627–633
6. Kurihara LJ, Kikuchi T, Wada K, Tilghman SM: Loss of Uch-L1 and Uch-L3 leads to neurodegeneration, posterior paralysis and dysphagia. Hum Mol Genet 2001, 10:1963–1970
7. Kurihara LJ, Semenova E, Levorse JM, Tilghman SM: Expression and functional analysis of Uch-L3 during mouse development. Mol Cell Biol 2000, 20:2498–2504
8. Saigoh K, Wang YL, Suh JG, Yamanishi T, Sakai Y, Kiyosawa H, Harada T, Ichihara N, Wakana S, Kikuchi T, Wada K: Intragenic deletion in the gene encoding ubiquitin carboxy-terminal hydrolase in gad mice. Nat Genet 1999, 23:47–51
9. Kon Y, Endoh D, Iwanaga T: Expression of protein gene product 9.5, a neuronal ubiquitin C-terminal hydrolase, and its developing change in Sertoli cells of mouse testis. Mol Reprod Dev 1999, 54:333–341
10. Wilkinson KD, Deshpande S, Larsen CN: Comparisons of neuronal (PGP 9.5) and non-neuronal ubiquitin C-terminal hydrolases. Biochem Soc Trans 1992, 20:631–637
11. Liu Y, Fallon L, Lashuel HA, Liu Z, Lansbury Jr PT: The UCH-L1 gene

encodes two opposing enzymatic activities that affect alpha-synuclein degradation and Parkinson's disease susceptibility. Cell 2002, 111:209–218
12. Liu Y, Lashuel HA, Choi S, Xing X, Case A, Ni J, Yeh LA, Cuny GD, Stein RL, Lansbury Jr PT: Discovery of inhibitors that elucidate the role of UCH-L1 activity in the H1299 lung cancer cell line. Chem Biol 2003, 10:837–846
13. Osaka H, Wang YL, Takada K, Takizawa S, Setsuie R, Li H, Sato Y, Nishikawa K, Sun YJ, Sakurai M, Harada T, Hara Y, Kimura I, Chiba S, Namikawa K, Kiyama H, Noda M, Aoki S, Wada K: Ubiquitin carboxy-terminal hydrolase L1 binds to and stabilizes monoubiquitin in neuron. Hum Mol Genet 2003, 12:1945–1958
14. Wada H, Kito K, Caskey LS, Yeh ET, Kamitani T: Cleavage of the C-terminus of NEDD8 by UCH-L3. Biochem Biophys Res Commun 1998, 251:688–692
15. Hemelaar J, Borodovsky A, Kessler BM, Reverter D, Cook J, Kolli N, Gan-Erdene T, Wilkinson KD, Gill G, Lima CD, Ploegh HL, Ovaa H: Specific and covalent targeting of conjugating and deconjugating enzymes of ubiquitin-like proteins. Mol Cell Biol 2004, 24:84–95
16. Gong L, Kamitani T, Millas S, Yeh ET: Identification of a novel isopeptidase with dual specificity for ubiquitin- and NEDD8-conjugated proteins. J Biol Chem 2000, 275:14212–14216
17. Harada T, Harada C, Wang YL, Osaka H, Amanai K, Tanaka K, Takizawa S, Setsuie R, Sakurai M, Sato Y, Noda M, Wada K: Role of ubiquitin carboxy terminal hydrolase-L1 in neural cell apoptosis induced by ischemic retinal injury in vivo. Am J Pathol 2004, 164:59–64
18. Kwon J, Wang YL, Setsuie R, Sekiguchi S, Sakurai M, Sato Y, Lee WW, Ishii Y, Kyuwa S, Noda M, Wada K, Yoshikawa Y: Developmental regulation of ubiquitin C-terminal hydrolase isozyme expression during spermatogenesis in mice. Biol Reprod 2004, 71:515–521
19. Boekelheide K, Hall SJ: 2,5-Hexanedione exposure in the rat results in long-term testicular atrophy despite the presence of residual spermatogonia. J Androl 1991, 12:18–26
20. Ohta Y, Nishikawa A, Fukazawa Y, Urushitani H, Matsuzawa A, Nishina Y, Iguchi T: Apoptosis in adult mouse testis induced by experimental cryptorchidism. Acta Anat (Basel) 1996, 157:195–204
21. Yin Y, Hawkins KL, DeWolf WC, Morgentaler A: Heat stress causes testicular germ cell apoptosis in adult mice. J Androl 1997, 18:159–165
22. Rasoulpour RJ, Schoenfeld HA, Gray DA, Boekelheide K: Expression of a K48R mutant ubiquitin protects mouse testis from cryptorchid injury and aging. Am J Pathol 2003, 163:2595–2603
23. Yin Y, DeWolf WC, Morgentaler A: Experimental cryptorchidism induces testicular germ cell apoptosis by p53-dependent and -independent pathways in mice. Biol Reprod 1998, 58:492–496
24. Peltola V, Huhtaniemi I, Ahotupa M: Abdominal position of the rat testis is associated with high level of lipid peroxidation. Biol Reprod 1995, 53:1146–1150
25. Ahotupa M, Huhtaniemi I: Impaired detoxification of reactive oxygen and consequent oxidative stress in experimentally cryptorchid rat testis. Biol Reprod 1992, 46:1114–1118
26. Morimoto RI, Santoro MG: Stress-inducible responses and heat shock proteins: new pharmacologic targets for cytoprotection. Nature Biotechnol 1998, 16:833–838
27. Wojcik C: Proteasomes in apoptosis: villains or guardians? Cell Mol Life Sci 1999, 56:908–917
28. Yang Y, Yu X: Regulation of apoptosis: the ubiquitous way. EMBO J 2003, 17:790–799
29. Kwon J, Kikuchi T, Setsuie R, Ishii Y, Kyuwa S, Yoshikawa Y: Characterization of the testis in congenitally ubiquitin carboxy-terminal hydrolase-1 (Uch-L1) defective (gad) mice. Exp Anim 2003, 52:1–9
30. Taylor CT, Furuta GT, Synnestvedt K, Colgan SP: Phosphorylation-dependent targeting of cAMP response element binding protein to the ubiquitin/proteasome pathway in hypoxia. Proc Natl Acad Sci USA 2000, 97:12091–12096
31. Park C, Choi WS, Kwon H, Kwon YK: Temporal and spatial expression of neurotrophins and their receptors during male germ cell development. Mol Cells 2001, 12:360–367
32. Finkbeiner S: CREB couples neurotrophin signals to survival messages. Neuron 2000, 25:11–14
33. Selvakumaran M, Lin HK, Miyashita T, Wang HG, Krajewski S, Reed JC, Hoffman B, Liebermann D: Immediate early up-regulation of bax expression by p53 but not TGF beta 1: a paradigm for distinct apoptotic pathways. Oncogene 1994, 9:1791–1798
34. Liu L, Cavanaugh JE, Wang Y, Sakagami H, Mao Z, Xia Z: ERK5 activation of MEF2-mediated gene expression plays a critical role in BDNF-promoted survival of developing but not mature cortical neurons. Proc Natl Acad Sci USA 2003, 100:8532–8537
35. Matsui Y: Regulation of germ cell death in mammalian gonads. APMIS 1998, 106:142–148
36. Gosden R, Spears N: Programmed cell death in the reproductive system. Br Med Bull 1997, 53:644–661
37. Print CG, Loveland KL: Germ cell suicide: new insights into apoptosis during spermatogenesis. Bioessays 2000, 22:423–430
38. Lee JC, Peter ME: Regulation of apoptosis by ubiquitination. Immunol Rev 2003, 193:39–47
39. Haupt Y, Maya R, Kazaz A, Oren M: Mdm2 promotes the rapid degradation of p53. Nature 1997, 387:296–299
40. Oren M: Regulation of the p53 tumor suppressor protein. J Biol Chem 1999, 274:36031–36034
41. Ryan KM, Phillips AC, Vousden KH: Regulation and function of the p53 tumor suppressor protein. Curr Opin Cell Biol 2001, 13:332–337
42. Dimmeler S, Breitschopf K, Haendeler J, Zeiher AM: Dephosphorylation targets Bcl-2 for ubiquitin-dependent degradation: a link between the apoptosome and the proteasome pathway. J Exp Med 1999, 189:1815–1822
43. Marshansky V, Wang X, Bertrand R, Luo H, Duguid W, Chinnadurai G, Kanaan N, Vu MD, Wu J: Proteasomes modulate balance among proapoptotic and antiapoptotic Bcl-2 family members and compromise functioning of the electron transport chain in leukemic cells. J Immunol 2001, 166:3130–3142
44. Suzuki Y, Nakabayashi Y, Takahashi R: Ubiquitin-protein ligase activity of X-linked inhibitor of apoptosis protein promotes proteasomal degradation of caspase-3 and enhances its anti-apoptotic effect in Fas-induced cell death. Proc Natl Acad Sci USA 2001, 98:8662–8667
45. Yin Y, Stahl BC, DeWolf WC, Morgentaler A: P53 and Fas are sequential mechanisms of testicular germ cell apoptosis. J Androl 2002, 23:64–70
46. Ohta H, Aizawa S, Nishimune Y: Functional analysis of the p53 gene in apoptosis induced by heat stress or loss of stem cell factor signaling in mouse male germ cells. Biol Reprod 2003, 68:2249–2254
47. Beumer TL, Roepers-Gajadien HL, Gademan IS, Lock TM, Kal HB, De Rooij DG: Apoptosis regulation in the testis: involvement of Bcl-2 family members. Mol Reprod Dev 2000, 56:353–359
48. Oldereid NB, Angelis PD, Wiger R, Clausen OP: Expression of Bcl-2 family proteins and spontaneous apoptosis in normal human testis. Mol Hum Reprod 2001, 7:403–408
49. Borner C: The Bcl-2 protein family: sensors and checkpoints for life-or-death decisions. Mol Immunol 2003, 39:615–647
50. Yamamoto CM, Sinha Hikim AP, Huynh PN, Shapiro B, Lue Y, Salameh WA, Wang C, Swerdloff RS: Redistribution of Bax is an early step in an apoptotic pathway leading to germ cell death in rats, triggered by mild testicular hyperthermia. Biol Reprod 2000, 63: 1683–1690
51. Deveraux QL, Reed JC: IAP family proteins—suppressors of apoptosis. Genes Dev 1999, 13:239–252
52. Yang Y, Fang S, Jensen JP, Weissman AM, Ashwell JD: Ubiquitin protein ligase activity of IAPs and their degradation in proteasomes in response to apoptotic stimuli. Science 2000, 288:874–877
53. Deveraux QL, Roy N, Stennicke HR, Van Arsdale T, Zhou Q, Srinivasula SM, Alnemri ES, Salvesen GS, Reed JC: IAPs block apoptotic events induced by caspase-8 and cytochrome c by direct inhibition of distinct caspases. EMBO J 1998, 17:2215–2223
54. Li B, Dou QP: Bax degradation by the ubiquitin/proteasome-dependent pathway: involvement in tumor survival and progression. Proc Natl Acad Sci USA 2000, 97:3850–3855
55. Semenova E, Wang X, Jablonski MM, Levorse J, Tilghman SM: An engineered 800 kilobase deletion of Uchl3 and Lmo7 on mouse chromosome 14 causes defects in viability, postnatal growth and degeneration of muscle and retina. Hum Mol Genet 2003, 12:1301–1312
56. Dil Kuazi A, Kito K, Abe Y, Shin RW, Kamitani T, Ueda N: NEDD8 protein is involved in ubiquitinated inclusion bodies. J Pathol 2003, 199:259–266

JOURNAL OF VIROLOGY, Feb. 2004, p. 2088–2099 Vol. 78, No. 4
0022-538X/04/$08.00+0 DOI: 10.1128/JVI.78.4.2088–2099.2004

Mutant PrP^{Sc} Conformers Induced by a Synthetic Peptide and Several Prion Strains

Patrick Tremblay,[1,2]†‡ Haydn L. Ball,[1,2]†§ Kiyotoshi Kaneko,[1]‖ Darlene Groth,[1] Ramanujan S. Hegde,[3]# Fred E. Cohen,[1,4,5] Stephen J. DeArmond,[1,3] Stanley B. Prusiner,[1,2,5]* and Jiri G. Safar[1,2]

Institute for Neurodegenerative Diseases[1] and Departments of Neurology,[2] Biochemistry and Biophysics,[5] Cellular and Molecular Pharmacology,[4] and Pathology,[3] University of California, San Francisco, California 94143

Received 6 August 2003/Accepted 15 October 2003

Gerstmann-Sträussler-Scheinker (GSS) disease is a dominantly inherited, human prion disease caused by a mutation in the prion protein (PrP) gene. One mutation causing GSS is P102L, denoted P101L in mouse PrP (MoPrP). In a line of transgenic mice denoted Tg2866, the P101L mutation in MoPrP produced neurodegeneration when expressed at high levels. $MoPrP^{Sc}$(P101L) was detected both by the conformation-dependent immunoassay and after protease digestion at 4°C. Transmission of prions from the brains of Tg2866 mice to those of Tg196 mice expressing low levels of MoPrP(P101L) was accompanied by accumulation of protease-resistant $MoPrP^{Sc}$(P101L) that had previously escaped detection due to its low concentration. This conformer exhibited characteristics similar to those found in brain tissue from GSS patients. Earlier, we demonstrated that a synthetic peptide harboring the P101L mutation and folded into a β-rich conformation initiates GSS in Tg196 mice (29). Here we report that this peptide-induced disease can be serially passaged in Tg196 mice and that the PrP conformers accompanying disease progression are conformationally indistinguishable from $MoPrP^{Sc}$(P101L) found in Tg2866 mice developing spontaneous prion disease. In contrast to GSS prions, the 301V, RML, and 139A prion strains produced large amounts of protease-resistant PrP^{Sc} in the brains of Tg196 mice. Our results argue that $MoPrP^{Sc}$(P101L) may exist in at least several different conformations, each of which is biologically active. Such conformations occurred spontaneously in Tg2866 mice expressing high levels of $MoPrP^{C}$(P101L) as well as in Tg196 mice expressing low levels of $MoPrP^{C}$(P101L) that were inoculated with brain extracts from ill Tg2866 mice, with a synthetic peptide with the P101L mutation and folded into a β-rich structure, or with prions recovered from sheep with scrapie or cattle with bovine spongiform encephalopathy.

The discovery that brain fractions enriched for prion infectivity contain a protein ($rPrP^{Sc}$) that is resistant to limited proteolytic digestion advanced prion research (8, 37). N-terminal truncation of $rPrP^{Sc}$ produced a protease-resistant fragment, denoted PrP 27-30, that is readily measured by Western blotting, enzyme-linked immunosorbent assay, or immunohistochemistry. The measurement of PrP^{Sc} was dramatically changed with the development of the conformation-dependent immunoassay (CDI), which permitted detection of full-length $rPrP^{Sc}$ as well as previously unrecognized protease-sensitive forms of PrP^{Sc} (39).

The CDI depends on using anti-PrP antibodies that react with an epitope exposed in native PrP^{C} but that do not bind to native PrP^{Sc}. Upon denaturation, the buried epitope in PrP^{Sc} becomes exposed and readily reacts with anti-PrP antibodies. Using the CDI, we discovered that most PrP^{Sc} is protease sensitive, which we designate $sPrP^{Sc}$. Whether $sPrP^{Sc}$ is an intermediate in the formation of $rPrP^{Sc}$ remains to be determined. In Syrian hamsters inoculated with eight different strains of prions, the ratio of $rPrP^{Sc}$ to $sPrP^{Sc}$ was different for each strain and the concentration of $sPrP^{Sc}$ was proportional to the length of the incubation time (39).

In earlier studies, transgenic (Tg) mice, denoted Tg2866, expressing high levels of PrP(P101L) were used to model Gerstmann-Sträussler-Scheinker (GSS) disease caused by the P102L point mutation. In the brains of several lines of mice expressing high levels of PrP(P101L), no $rPrP^{Sc}$(P101L) was detectable (26, 27, 47). This was particularly perplexing since these Tg mice expressing high levels of PrP(P101L) developed all facets of prion-induced neurodegeneration, including multicentric PrP amyloid plaques. Moreover, brain extracts from ill Tg2866 mice transmitted disease to Tg196 mice expressing low levels of PrP(P101L) that infrequently developed spontaneous neurodegeneration (29).

In humans with GSS, several different mutations of the PrP gene (*PRNP*) resulting in nonconservative amino acid substitutions have been identified (23). In these patients, the clinical presentation, disease course, and amounts of $rPrP^{Sc}$ in the brain are variable. Brain extracts from humans who died of GSS were inoculated into apes and monkeys, but the transmission rates were not correlated with the levels of PrP^{Sc} in the inoculum (1, 2, 9, 32). In a limited study, GSS(P102L) was transmitted to Tg mice expressing a chimeric mouse-human (MHu2 M) PrP transgene carrying the P102L mutation but not

* Corresponding author. Mailing address: Institute for Neurodegenerative Diseases, University of California, Box 0518, San Francisco, CA 94143-0518. Phone: (415) 476-4482. Fax: (415) 476-8386. E-mail: stanley@itsa.ucsf.edu.

† These authors contributed equally to this work.

‡ Present address: Neurochem Inc., St. Laurent, QC H4S 2A1, Canada.

§ Present address: University of Texas Southwestern Medical Center, Dallas, TX 75390.

‖ Present address: National Center of Neurology and Psychiatry and Core Research for Evolutional Science and Technology, Kodaira, Tokyo 187-8502, Japan.

Present address: National Cancer Institute, Bethesda, MD 20892.

TABLE 1. Characteristics of PrP(P101L) isoforms

Characteristic	Isoform[a]		
	PrP^{c}(P101L)	$sPrP^{Sc}$(P101L)	$rPrP^{Sc}$(P101L)
PrP epitopes (residues 90–125) in native state	Exposed	Buried	Buried
Precipitatable by PTA	−	+	+
Digestion with PK at 37°C ("PK")	Dipeptides, tripeptides	Dipeptides, tripeptides	PrP 27–30
Digestion with PK at 4°C ("cold PK")	Dipeptides, tripeptides	PrP 22–24	PrP 27–30
Infectious	−	?	+

[a] ?, unknown; +, positive; −, negative.

to Tg mice expressing MHu2M PrP without the mutation (47). In another study, GSS(P102L) human prions were transmitted to Tg mice expressing MoPrP(P101L) in which the transgene was incorporated through gene replacement (31). The use of gene replacement permits all of the regulatory elements that control the wild-type (wt) MoPrP gene to modulate the expression of MoPrP(P101L). In these mice, the expression level of MoPrP(P101L) in brain is likely to be similar to that in Tg196 mice.

When we synthesized a 55-mer MoPrP peptide composed of residues 89 to 143 containing the P101L mutation and folded it under conditions favoring a β-structure, it induced neurodegeneration in Tg196 mice (29). When the peptide was not folded into a β-structure, it did not produce disease in Tg196 mice. We report here that the peptide-initiated disease in Tg196 mice could be serially transmitted to other Tg196 mice using brain extracts from the peptide-inoculated Tg196 mice. Using procedures derived from the CDI, brain extracts from inoculated Tg196 mice were found to contain $sPrP^{Sc}$(P101L), from which a 22- to 24-kDa PrP fragment was generated by limited digestion with proteinase K (PK) at 4°C and selective precipitation with phosphotungstate (PTA) (25, 39). In the interest of clarity, we have designated digestion at 4°C as "cold PK" and simply refer to standard digestion at 37°C as "PK." To aid in distinguishing $rPrP^{Sc}$(P101L) from $sPrP^{Sc}$(P101L), their properties based on the work reported here and in other previously published papers are listed in Table 1 (39, 40).

In addition to inoculating Tg196 mice with brain extracts containing $sPrP^{Sc}$(P101L) or with the MoPrP(89-143,P101L) peptide, we inoculated Tg196 with several strains of prions carrying wt $MoPrP^{Sc}$-A or $MoPrP^{Sc}$-B. The 301V strain carrying wt $MoPrP^{Sc}$-B (22) exhibited similar abbreviated incubation times in both Tg196 mice and $Prnp^{b/b}$ mice. In contrast, the RML and 139A strains carrying wt $MoPrP^{Sc}$-A showed prolonged incubation times in both Tg196 and $Prnp^{b/b}$ mice (12, 33). Regardless of the host mouse strain, the 301V, RML, and 139A prion strains produced large amounts of $rPrP^{Sc}$ in the brains of inoculated mice. Thus, the discovery of $sPrP^{Sc}$ has for the first time provided a molecular signature for GSS prions that either arise spontaneously in mice or are induced by a synthetic peptide carrying the GSS mutation.

MATERIALS AND METHODS

Source of laboratory animals. The results reported here were derived from studies using Tg(MoPrP,P101L)196/$Prnp^{0/0}$, Tg(MoPrP,P101L)2866/$Prnp^{0/0}$, Tg(MoPrP,P101L)2247/$Prnp^{0/0}$, Tg(MoPrP)4053/$Prnp^{+/+}$, Tg(MHu2M)5378/$Prnp^{0/0}$, and Tg(MHu2MPrP,P102L)69/$Prnp^{0/0}$ mice; these Tg lines are described in detail elsewhere (27, 47, 48). All PrP-deficient animals originated from Zrch $Prnp^{0/0}$ mice (11). Transgenic lines were maintained by breeding with FVB $Prnp^{0/0}$, except for Tg(MoPrP)4053/$Prnp^{+/+}$, in which the endogenous *Prnp* gene was maintained by breeding with FVB mice (Charles River Laboratories, Hollister, Calif.). Swiss CD-1 mice, which express $Prnp^{a}$, were obtained from Charles River Laboratories, and B6.I mice, which express $Prnp^{b}$, were a generous gift from G. Carlson (12). Rabbits were obtained from Western Oregon Rabbit Company (Philomath, Ore.).

Transmission studies. The RML prion strain was derived from the Chandler isolate (14) passaged in CD-1 mice. The mouse 139A prion strain, originally isolated after more than 20 passages in mice, was obtained from R. Carp (21) and serially propagated in C57BL ($Prnp^{a/a}$) mice obtained from Charles River Laboratories. The 301V prion strain, originally isolated from a cow infected with bovine spongiform encephalopathy (BSE), was obtained from H. Fraser (10) and maintained by serial passaging in B6.I mice. Brains from ill, MoPrP(89-143, P101L) peptide-inoculated Tg196 mice were obtained from previously reported experiments (29). Ten-percent (wt/vol) brain homogenates (BH) were obtained by 10 serial extrusions through 18-, 20-, and 22-gauge needles in phosphate-buffered saline (PBS) (pH 7.4). Mice were inoculated intracerebrally (i.c.) with 30 μl of 1% BH (Table 2) or with a clarified 0.5% BH (Table 3) using a 27-gauge, disposable hypodermic syringe. Alternatively, following PTA precipitation of 1 ml of BH, pellets were resuspended in 500 μl of diluent (PBS) before i.c. inoculation (Table 3). Disease diagnosis was carried out biweekly, and animals were sacrificed following evidence of progressive neurologic dysfunction (13, 41).

Treatment of brain homogenates. For biochemical analysis only, 10% BH samples were prepared in Ca^{++}- and Mg^{++}-free PBS by homogenization (three strokes of 15 s each) with a PowerGen 125 homogenizer (Fisher Scientific). Homogenates were clarified by centrifugation at 500 × *g* for 5 min on a tabletop centrifuge. Supernatants were subjected to cold PK or PK digestion alone or in conjunction with PTA precipitation. For PK digestion, 5% BH samples were incubated with 25 μg of PK (Gibco BRL no. 25530-015; Invitrogen, Carlsbad, Calif.)/ml for 1 h at 37°C. PK activity was blocked using a protease inhibitor (PI) cocktail composed of 2 μg of aprotinin and leupeptin/ml and 0.2 mM phenylmethylsulfonyl fluoride. For cold PK digestion, clarified 10% BH containing 1% NP-40 was incubated with 250 μg of PK/ml for 1 h on ice. Samples were treated with PI (200 μg of aprotinin and leupeptin/ml and 5 mM phenylmethylsulfonyl fluoride), transferred to five volumes of preheated PK inactivation buffer (1% sodium dodecyl sulfate [SDS], 0.1 M Tris-HCl [pH 8.9]), and incubated at 100°C for 2 min. For cold PK followed by PTA precipitation, 10% BH were treated with cold PK, and the reaction was blocked using PI. Samples were diluted with one volume of PBS–4% Sarkosyl and PTA precipitated. For ultracentrifugation, 1 ml of these samples was centrifuged at 100,000 × *g* for 1 h at 4°C. Alternatively, 1 ml was precipitated with PTA by adjusting samples to 0.3% PTA–2.5 mM $MgCl_2$, incubated at 37°C for 1 h, and centrifuged at 16,000 × *g* for 30 min. Pellets were resuspended in PBS with PI and 0.2% Sarkosyl.

For Western blot analysis, samples were diluted with one volume of 0.1 M Tris (pH 6.8)–2% mercaptoethanol–2% NP-40 and subjected to 7.2 U of PNGase F1 per 100 μg of total protein at 37°C overnight, according to the manufacturer's recommendations (Boehringer-Mannheim, Mannheim, Germany). Proteins were precipitated with 25% trichloroacetic acid and washed with acetone. Pellets were resuspended in 1% SDS–0.1 M Tris-HCl (pH 8.9) buffer for loading on an SDS polyacrylamide gel.

Immunological reagents. To take advantage of the CDI and characterize the conformational transitions associated with PrP(P101L), we sought to identify antibodies that recognize epitopes in the region of MoPrP(P101L) located between residues 89 and 143. Surprisingly, all previously described candidate antibodies for this assay (including recombinant fragment antibody D13 [35] and polyclonal antiserum 9095 [42]), which recognize wt MoPrP within these boundaries, poorly recognized MoPrP(P101L) by Western blotting (data not shown). Therefore, a polyclonal antiserum was raised in rabbits using a random-coil